ADVANCED FUNCTIONAL MATERIALS
www.afm-journal.de

Critical Challenges and Optimization Strategies for Rechargeable Aluminum-Sulfur Batteries

Yu Wang, Xiaolin Wu, Jiashen Meng, Hao Zhang, Yibo Song, Xuanpeng Wang, Yakun Liu, and Liqiang Mai**

The increasing demand for efficient, cost-effective energy storage systems has spurred research into alternatives to lithium-ion batteries. Among these alternatives, aluminum-sulfur (Al-S) batteries have become a promising option, demonstrating noteworthy advancements over the past decade. These batteries provide benefits such as high theoretical energy density, low cost, and improved safety. Nonetheless, certain fundamental electrochemical challenges, similar to those encountered by other sulfur-based batteries, persist, including slow reaction kinetics, significant polysulfide shuttling, and uncontrollable dendrite growth on the anode. Herein, this review offers a comprehensive overview of recent advancements related to the critical challenges and optimization strategies for rechargeable Al-S batteries. It begins by outlining the development history of Al-S batteries and the challenges present in current systems. Next, efficient optimization strategies aimed at enhancing Al-S batteries are summarized by focusing on optimizing each battery component, including the cathode, anode, electrolyte, and separator. Detailed examinations include structural features, electrochemical performance, structure-property correlations, and enhancement mechanisms of key breakthroughs. Finally, the challenges and potential opportunities are explored for future research on rechargeable Al-S batteries. This review aims to provide insightful guidance for the rational design of high-performance Al-S batteries and to accelerate their development for practical large-scale energy storage applications.

1. Introduction

The urgent need for sustainable energy alternatives to traditional fossil fuels has arisen due to the escalating energy crisis and environmental pollution.[1–3] Although renewable energy technologies like wind, hydropower, solar, and biomass present viable alternatives, their inherent intermittency and unpredictability create substantial barriers to widespread adoption.[4] Advancing large-scale electrochemical energy storage systems is viewed as a critical strategy for addressing the limitations of these clean energy sources and facilitating their efficient use.[5–7] Although lithium-ion batteries have been commercially viable since the 1990s, yet researchers now concentrate on novel energy storage technologies that promise lower costs, improved safety, and higher energy densities.[8,9] This shift is motivated by concerns over the depletion of lithium resources, the volatility of lithium prices, and safety issues related to existing lithium-ion battery technology.[10]

As illustrated in **Figure 1a**, although the redox potential of the Al^{3+}/Al pair is higher than that of the Li^+/Li, Na^+/Na, K^+/K, Mg^{2+}/Mg, and Ca^{2+}/Ca pairs, aluminum-based batteries offer a volumetric capacity of 8046 mAh cm^{-3}, which is four-fold greater than that of lithium metal.[11] Furthermore, the theoretical weight capacity of aluminum is 2980 mAh g^{-1}, comparable to that of lithium. Additionally, aluminum outperforms other metal battery systems regarding safety and resource availability.[12–15] Aluminum-ion batteries possess substantial potential for large-scale energy storage applications.[16–20] Cathodes

Y. Wang, X. Wu, J. Meng, H. Zhang, Y. Song, L. Mai
State Key Laboratory of Advanced Technology for Materials Synthesis and Processing
School of Materials Science and Engineering
Wuhan University of Technology
Wuhan 430070, P. R. China
E-mail: jsmeng@whut.edu.cn; mlq518@whut.edu.cn

X. Wu
School of Chemical Engineering
Zhengzhou University
Zhengzhou 450001, P. R. China

J. Meng, X. Wang
Zhongyu Feima New Material Technology Innovation Center (Zhengzhou) Co., Ltd
Zhengzhou, Henan 450001, P. R. China

X. Wang
Department of Physical Science & Technology
School of Physics and Mechanics
Wuhan University of Technology
Wuhan 430070, P. R. China

Y. Liu
Department of Electric Engineering
Shanghai Jiao Tong University
Shanghai 200240, P. R. China

The ORCID identification number(s) for the author(s) of this article can be found under https://doi.org/10.1002/adfm.202423454

DOI: 10.1002/adfm.202423454

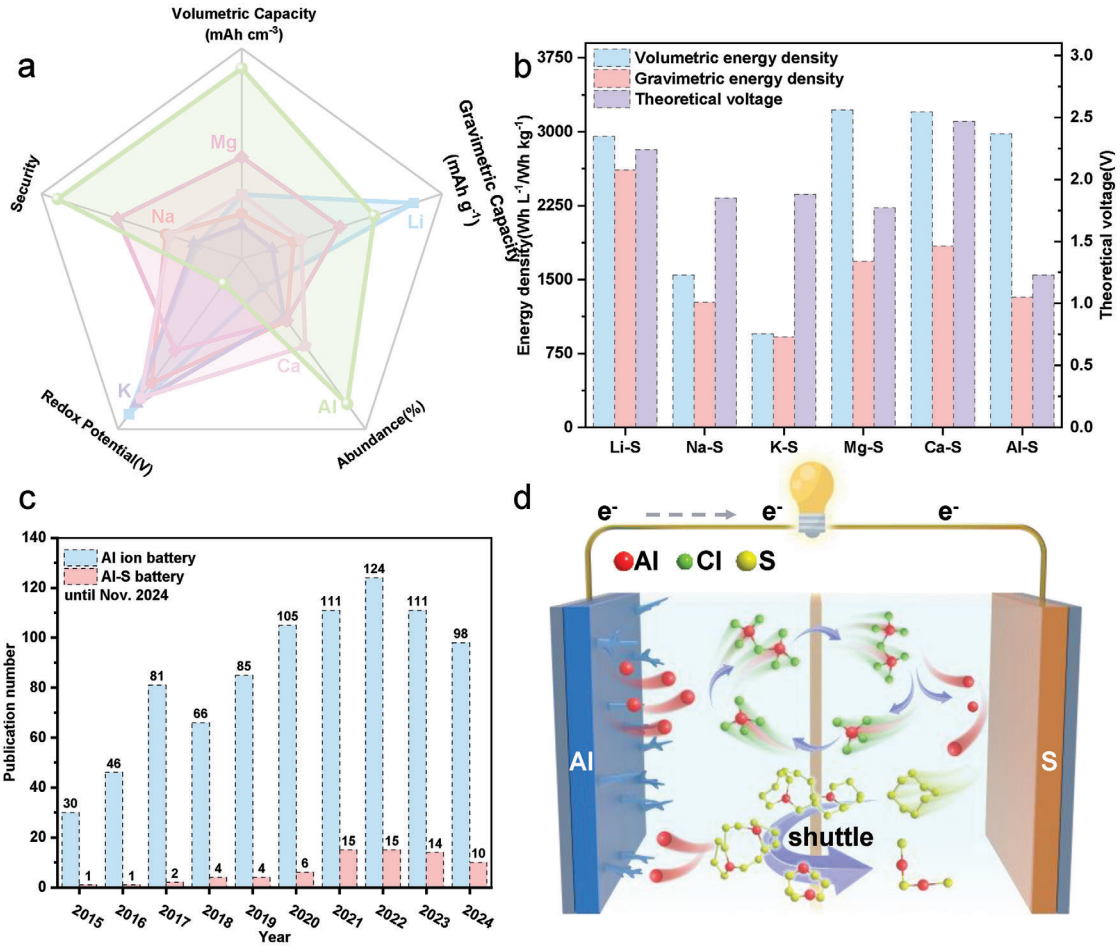

Figure 1. a) Five important indicators of Al, Li, Na, K, Mg, and Ca metal anodes in energy storage systems. b) Theoretical volumetric/gravimetric energy densities and voltage of Li-S, Na-S, K-S, Mg-S, Ca-S, and Al-S batteries. c) Number of publications of rechargeable Al ion batteries and Al-S batteries searched from "Web of Science". d) Schematic representation view of the Al–S battery.

in these batteries can be classified into two types based on their electrochemical mechanisms: intercalation-type and conversion-type.[21–23] The conversion-type cathode, which uses elemental sulfur, is especially appealing due to its low cost, high theoretical specific capacity of 1675 mAh g^{-1}, and environmental friendliness, positioning aluminum-sulfur (Al-S) batteries as strong contenders in the evolving energy storage landscape.[24–27] Whether in the field of static or dynamic energy storage, this system battery can well meet the energy storage needs of various scenarios. In particular, the high energy/price ratio makes it stand out among many metal-sulfur energy storage systems and plays an irreplaceable role. As illustrated in Figure 1b, the theoretical volumetric energy density of Al-S batteries is 2981 Wh L^{-1}. This value is comparable to that of Li-S batteries at 2955 Wh L^{-1}, slightly lower than Mg-S batteries at 3221 Wh L^{-1} and Ca-S batteries at 3202 Wh L^{-1}, and significantly higher than Na-S batteries at 1545 Wh L^{-1} and K-S batteries at 952 Wh L^{-1}.[28–34]

As early as the 1970s, researchers began to study Al-S batteries. As shown in Figure 1c, it was not until 2015 that researchers reported Al-graphene batteries based on ionic liquids with excellent stability, and Al-S batteries entered a development period. In recent years, there are more than 15 reports on Al-S batteries each year. Figure 1d illustrates a schematic representation of a typical Al-S battery. Al-S batteries generally consist of an ionic liquid (IL), molten salt, or water-based electrolyte, using aluminum foil as the anode and a conductive substrate loaded with sulfur—such as conductive carbon black or a metal network—as the cathode.[35,36] Most current Al-S batteries utilize room-temperature IL made from $AlCl_3$ and chlorinated 1-methyl-3-ethylimidazolium cations (EMIMCl). This mixture remains liquid at room temperature due to acid-base interactions, where $AlCl_3$ functions as a Lewis acid and Cl^- serves as a Lewis base. When the proportion of $AlCl_3$ exceeds that of EMIMCl, the IL mainly consists of $AlCl_4^-$ and $Al_2Cl_7^-$.[37] In Al-S batteries that utilize this IL electrolyte, researchers generally propose that the following reactions take place during the electrochemical redox process:[35,38–42]

$$\text{Aluminum Anode}: 2Al + 14AlCl_4^- \rightarrow 8Al_2Cl_7^- + 6e^- \quad (1)$$

$$\text{Sulfur Cathode}: 4Al_2Cl_7^- \rightarrow 7AlCl_4^- + Al^{3+} \quad (2)$$

$$2Al^{3+} + 6e^- + 3S \rightarrow Al_2S_3 \quad (3)$$

$$\text{Overall}: 2Al + 3S \leftrightarrow Al_2S_3 \quad (4)$$

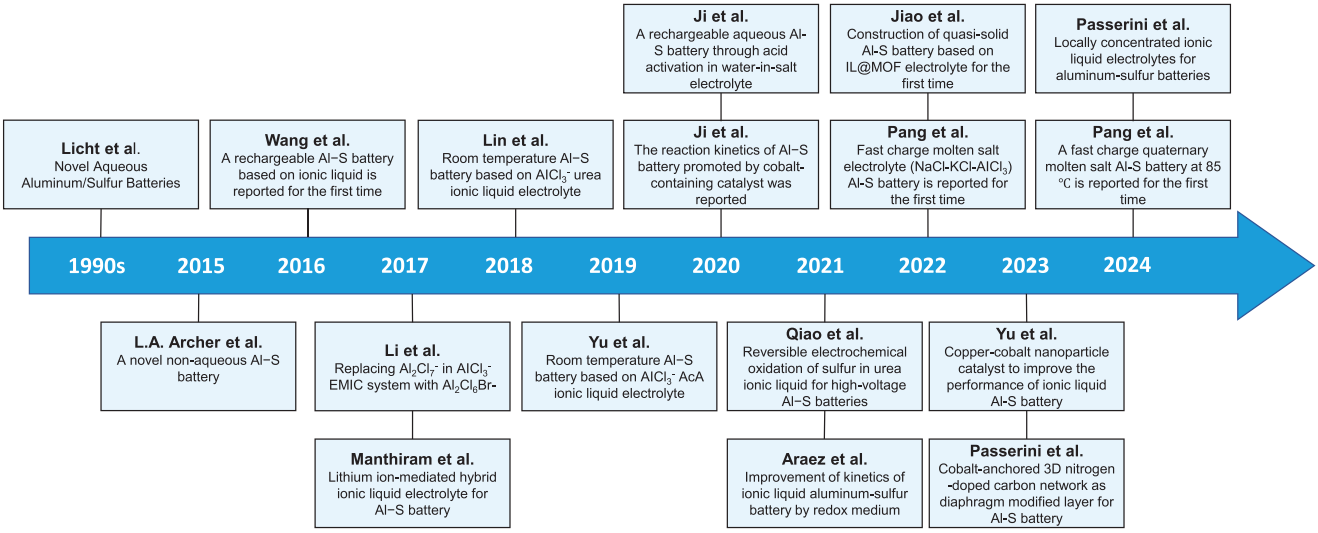

Figure 2. Schematic diagram of the historical development of Al-S batteries.

During the discharge process, as illustrated in Equation (1), an oxidation reaction takes place between the aluminum anode and $AlCl_4^-$, resulting in the formation of $Al_2Cl_7^-$. This compound is then electrochemically transported across the diaphragm to the positive side, where it interacts with sulfur. Under the influence of an electric field, $Al_2Cl_7^-$ dissociates, releasing Al^{3+} ions, as shown in Equation (2). These Al^{3+} ions react with sulfur, reducing it to aluminum polysulfides (AlPSs) and sulfides, similar to the sulfur transformations observed in lithium-sulfur (Li-S) batteries. Initially, the reaction between sulfur (S_8) and Al^{3+} produces long-chain Al_2S_{18}, which subsequently transforms through various polysulfide intermediates, such as Al_2S_{12} and Al_2S_6, ultimately converting to Al_2S_3, as detailed in Equation (3). The overall electrochemical reaction of the battery is outlined in Equation (4).

The minimal intrinsic electronic conductivity of sulfur (5×10^{-30} S cm^{-1}) and its substantial volumetric change of ≈80% during the electrochemical process can lead to low sulfur utilization and potential structural damage in the cathode, negatively affecting the battery's capacity and lifespan.[42] Similarly, the use of IL electrolytes can negatively impact the aluminum anode due to corrosion at the interface, slow reaction kinetics, and irregular deposition during cycling. These issues can result in increased polarization and decreased cycling stability, ultimately shortening the battery's lifespan.[43,44] The metal-sulfur battery system suffers from the polysulfide shuttle effect, causing the deposition of both soluble polysulfides (Al_2S_n) and insoluble sulfides (Al_2S_3) on the anode. This phenomenon reduces the sulfur utilization rate and diminishes the battery's capacity. Moreover, the multistep electrochemical reactions in steps (2) and (3) are obstructed by a high potential barrier, negatively affecting the reaction kinetics of the Al-S battery. Additionally, the accumulation of insoluble sulfides on the electrode surface impedes the transport of aluminum ions, thereby reducing the battery's performance.[45,46]

This review presents an in-depth analysis of recent advancements addressing the primary challenges and optimization strategies for rechargeable Al-S batteries. First, the historical development and primary challenges of Al-S batteries are summarized. It systematically investigates recent research advancements aimed at developing efficient strategies for optimizing reaction kinetics, inhibiting polysulfide shuttle effects, and safeguarding the aluminum anode interface. These strategies focus on various components of the battery, including cathode material design, electrolyte optimization, separator modifications, and surface modifications of the aluminum anode. Furthermore, the review identifies challenges and future directions for advancing practical Al-S batteries, aiming to develop a high-specific-energy storage system that is both mature and relevant for real-world applications.[47,48]

2. Status and Challenges of Al-S Batteries

2.1. Historical Progress

Sulfur electrodes are of significant interest owing to their affordability and elevated theoretical capacity (**Figure 2**). The electrochemical properties of sulfides in $AlCl_3$-NaCl melts were first explored in the 1970s by Maeassi et al.[49–51] In the 1990s, Peramunage et al. developed the inaugural Al-S battery using an aqueous electrolyte.[52,53] However, progress stalled for two decades until 2015, when Archer et al. introduced a Non-rechargeable non-aqueous Al-S battery utilizing an IL substrate.[54] This innovation achieved a capacity exceeding 1400 mAh g^{-1} by replacing the sulfur cathode after each cycle in a specialized cylindrical device, maintaining performance over multiple cycles without significant potential drop or capacity loss. In 2016, Wang et al. at the University of Maryland pioneered an Al-S battery with an activated carbon cloth/sulfur cathode and an IL electrolyte composed of $AlCl_3$ and chlorinated 1-methyl-3-ethylimidazole.[38] This battery demonstrated nearly 100% Coulombic efficiency with a discharge voltage of ≈0.65 V at a current density of 50 mA g^{-1} and sustained a capacity of 1000 mAh g^{-1} after 20 cycles. Al-S batteries have recently experienced rapid development, attracting significant scholarly attention owing to their potential as affordable, high-capacity energy storage solutions. Researchers have focused on optimizing electrolyte modifications, cathode

design, and diaphragm strategies. For instance, Manthira et al. enhanced the cycling performance and minimized polarization in Al-S batteries by applying single-walled carbon nanotubes (SWCNTs) to the diaphragm.[55] They also proposed an electrochemical process utilizing a conventional IL electrolyte. During the charge–discharge cycles, various polysulfides, and sulfides are formed, with higher-order polysulfides (S_x^{2-}, where $x \geq 6$) dissolving within the IL electrolyte. Reversible transformations occur between S_6^{2-} and insoluble lower-order polysulfides or sulfides, while the diaphragm modification strategy effectively mitigates the shuttle effect of higher-order polysulfides. Similarly, a 3D nitrogen-doped carbonaceous network anchored with cobalt ($Co@C_{Mel\text{-}ZIF}$) prepared by carbonizing a mixture of ZIF-7, melamine, and $CoCl_2$ as a modified diaphragm can effectively alleviate the high polarization of Al-S batteries and improve cycle performance.[56]

In optimizing the electrolyte, Li et al. team reduced the dissociation energy barrier of long-chain chloroaluminate by substituting $Al_2Cl_7^-$ with $Al_2Cl_6Br^-$ in the IL electrolyte.[57] This substitution increased the dissociation reaction rate by 15-fold, as determined by the Arrhenius equation, significantly enhancing the reaction kinetics of the Al-S battery. Similarly, a Li^+-ion-mediated IL optimization strategy was implemented to enhance the stability of Al-S battery by promoting sulfide conversion.[58] In recent years, the Araez et al. team found that by introducing a low concentration of redox medium in the electrolyte system, the charging voltage platform of the Al-S battery can be significantly reduced, the dynamics of the Al-S battery can be improved, and the electrochemical reaction process of the catalytic system can be improved.[59] Passerini et al. proposed a locally concentrated IL electrolyte formed by diluting the IL with a non-solvated 1, 2-difluorobenzene co-solvent, which effectively promoted the mobility and ionic conductivity and facilitated the reaction kinetics of the Al-S cell.[60] Subsequently, urea- and acetamide-based IL electrolytes with different ion coordination, aqueous electrolytes based on salt-in-water strategy, and quasi-solid-state IL@MOF electrolytes have further enriched the research in the field of Al-S battery electrolytes.[61–64] These diverse electrolytes reduce costs and expand beyond the sulfur reduction reaction in the low-voltage domain, bringing the sulfur oxidation reaction in the high-voltage domain into focus.[39,65] Investigating the sulfur oxidation pathway is crucial for designing high-voltage Al-S batteries, offering significant advantages and promising prospects.

To address the poor conductivity and low conversion of cathode sulfur, the cathode is often combined with a conductive substrate, typically carbon. To enhance sulfur utilization, structural design, and catalyst loading are frequently employed. Incorporating $Co^{II,III}$ into the carbon substrate of the cathode markedly enhances its conversion or catalytic effect on sulfur electrochemistry, thereby improving the reaction kinetics of Al-S batteries and sulfur utilization.[66] In recent years, Yu et al. have reported nitrogen-doped carbon-based composite materials containing copper and cobalt nanoparticles, which can effectively adsorb and convert polysulfides. After 320 cycles at 1.5 A g^{-1}, the Al-S battery can maintain a capacity of 317.5 mAh g^{-1}.[67]

Our group recently introduced a high-safety, cost-effective molten salt Al-S battery with remarkable fast-charging capabilities (up to 200 C) and cycling stability.[40] This innovation enables sulfur, a transformational electrode material based on full lattice reconstruction, to achieve fast-charging performance akin to traditional embedded materials. The use of a ternary inorganic chloride molten electrolyte, instead of the conventional IL electrolyte, facilitates the battery's high-rate operation, low voltage polarization, high energy efficiency, thermal stability, and safety. Furthermore, a fast-charging Al-S battery using an entropy-increasing quaternary chloroaluminate electrolyte at a sub-boiling water temperature of 85 °C was reported.[68] The battery maintained 85.4% of its capacity following 1400 cycles at 1 C charging rate. In situ, synchrotron radiation near-edge absorption spectroscopy and other methods were used to reveal the asymmetric sulfur reaction mechanism involving the generation of polysulfide intermediates.

Furthermore, theoretical simulation calculations have been employed to investigate the reaction mechanisms underlying the electrochemical processes in Al-S batteries. Pathak et al. team at the Indian Institute of Technology utilized molecular dynamics simulations to analyze the charge–discharge processes in IL Al-S batteries. Their findings revealed a gradual reduction mechanism of S_8 during discharge, involving the formation of various cationic and anionic intermediates, which subsequently drive the generation of AlPSs. Additionally, they observed the dissolution of AlPSs during the discharge process.[69] Similarly, Lastra et al. team developed a mathematical model to examine the distinct discharge mechanisms of IL Al-S batteries and the formation pathways of Al_2S_3 under varying discharge densities. Their study demonstrated that the reversibility of Al-S batteries, based on Al_2S_3 formation, is significantly influenced by the operating current density.[70] Subsequently, the group constructed a computational model from the perspective of ion coordination to investigate the impact of different ion coordination environments on the reaction mechanisms of Al-S batteries. Their predictions regarding the charge–discharge behavior of these batteries indicated that the most stable polysulfides exist in the form of coordination complexes.[71]

2.2. Challenges

Despite extensive research on Al-S battery systems, key scientific challenges remain in achieving practical applications (**Figure 3**). Currently, all reported Al-S batteries rely on conversion reactions and encounter several key problems:

1) Al-S battery systems have extremely slow reaction kinetics during cycling. From the perspective of positive electrode materials, the extremely poor conductivity of sulfur determines that it cannot be used alone as the cathode material for Al-S batteries. In fact, the composite of carbon materials with higher conductivity has made up for this defect to a certain extent. However, considering that the battery reaction involves a "solid-liquid-solid" three-phase conversion mechanism, this long-path conversion mode is obviously not conducive to the goal of building a fast-charging and efficient Al-S battery. Even more sad is that the multi-step redox reaction of Al-S batteries makes the battery suffer from high reaction kinetic barriers as a whole. In terms of electrolytes, due to the high reaction energy barrier of chloroaluminate ion clusters when removing Al^{3+}, the slow solvation and desolvation process of Al^{3+} in the

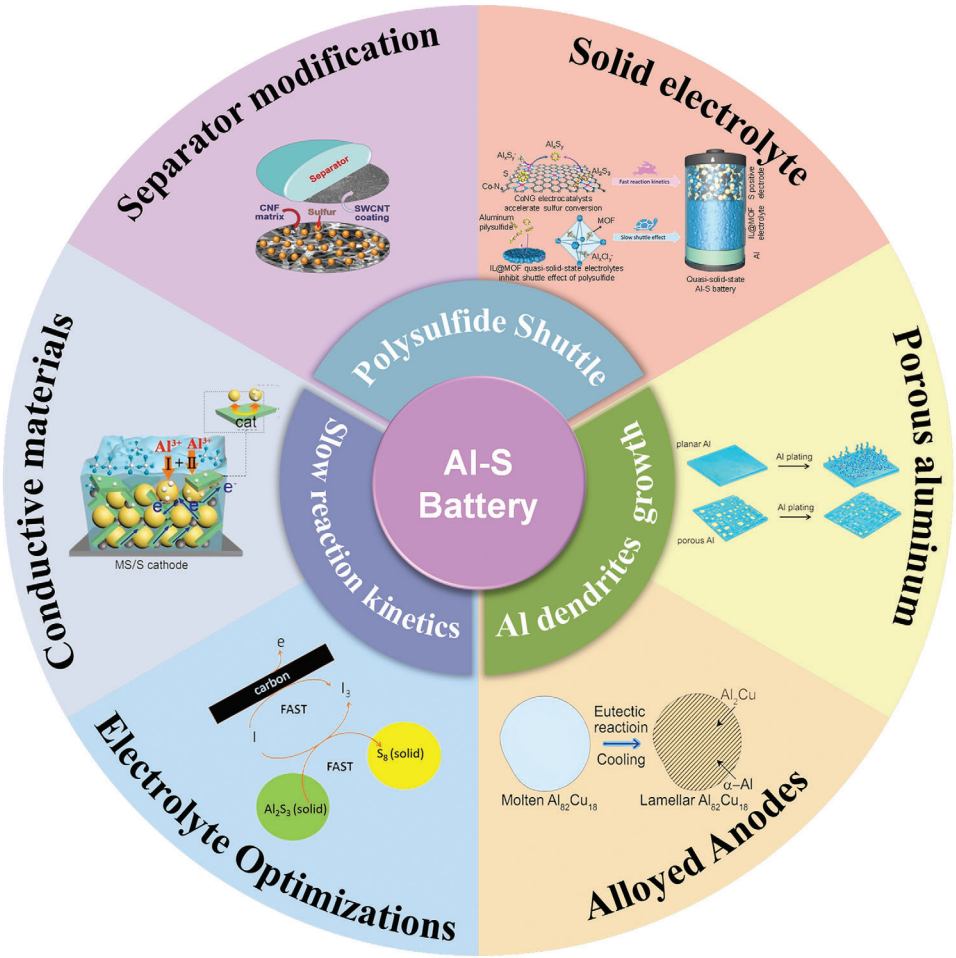

Figure 3. Challenges and solutions for Al-S batteries.

electrolyte is also considered to be one of the reasons for the slow reaction kinetics of the battery.

2) Al-S battery systems suffer from severe AlPSs shuttling during cycling. In the currently commonly used IL electrolytes, the sulfur/carbon composite positive electrode and its redox products all show serious dissolution phenomena. The dissolved sulfur species will use the electrolyte as a medium, traverse the separator, and deposit on the Al anode side. This unidirectional migration is regarded as the "Shuttle effect". On the one hand, this phenomenon leads to the depletion of active sulfur, resulting in battery capacity decline and low coulombic efficiency. On the other hand, the shuttled sulfur species also seriously contaminate the Al negative electrode, thereby greatly reducing the battery life.
3) Dendrite short circuit problem in Al-S battery system. During the (dis-)charge cycle of Al-S batteries, the duration of reversible plating/stripping varies depending on the actual situation. Under relatively large current density, the deposition of Al^{3+} on the surface of the Al negative electrode suffers from great uncertainty. Once the deposition rate is too fast and the local current density is too large, sharp Al dendrites may grow on the negative electrode surface. These dendrites will pierce the separator and cause battery failure. The following sections list some representative practices to address these challenges.

3. Kinetics Optimization Strategies

Elemental sulfur is a cost-effective by-product of the chemical industry and possesses a high theoretical capacity, making it a subject of intensive research as a cathode material for Al-S batteries. Significant progress has been achieved in understanding the redox reaction mechanisms, designing sulfur cathodes, and formulating electrolytes, which have collectively enhanced battery performance. However, the slow electrochemical reaction kinetics presents a formidable obstacle to the commercialization of Al-S batteries. This challenge largely arises from sulfur's naturally low electronic conductivity, which increases kinetic energy barriers during the conversion processes. Moreover, in traditional Al-S batteries, the conversion of sulfur to aluminum sulfide (Al_2S_3) occurs through a solid-liquid-solid reaction pathway. Initially, sulfur (S_8) transforms into long-chain Al_2S_{18}, which then undergoes further reactions with polysulfide intermediates like Al_2S_{12} and Al_2S_6, before ultimately yielding Al_2S_3. Each step of this process is impeded by significant kinetic energy barriers, leading to the accumulation of sulfur species and diminishing overall

conversion efficiency. Furthermore, the high solubility of long-chain polysulfides in the electrolyte undermines cycling stability. Current research predominantly centers on IL electrolytes for Al-S batteries, which face challenges such as poor kinetics and a restricted voltage range. These limitations result in suboptimal sulfur utilization and adversely affect the deposition of aluminum anodes, frequently causing battery failure during prolonged cycling. To overcome these challenges, researchers are investigating innovative designs for cathode conductive networks, optimizing electrolytes, and developing high-voltage Al-S batteries that leverage sulfur oxidation reactions. The next section will present key studies that address these critical issues.

3.1. Cathode Design

To overcome the limitations of sulfur as a conversion cathode, it is essential to achieve uniform dispersion of sulfur within a conductive substrate to facilitate electron transfer. Conductive carbon materials, known for their exceptional electrical conductivity, expansive specific surface area, and abundant pore space, greatly enhance the charge transfer capability of sulfur cathodes while simultaneously reducing sulfur solubility in the electrolyte. Early research primarily focused on basic carbon materials as conductive substrates for sulfur cathodes.[78–80] In the pioneering non-aqueous Al-S battery utilizing an IL electrolyte, Archer et al. selected Ketjen black carbon as the conductive substrate. The high specific surface area and effective adsorption properties of this material enabled uniform distribution of sulfur particles. Experimental results demonstrated that this cathode attained a remarkable specific capacity of 1400 mAh g^{-1} by replacing the sulfur cathode at a current density of 30 mA g^{-1}. Wang et al. pioneered the use of an IL as the electrolyte in a room-temperature rechargeable Al-S battery, employing activated carbon cloth (ACC) with sulfur uniformly loaded via a melt-diffusion as the cathode material. The Brunnauer–Emmett–Teller (BET) analysis revealed that the carbon material features a microporous structure with pore diameters less than 2 nm. Following sulfur loading, the specific surface area reduced from 2376.6 to 1532.8 m^2 g^{-1}, and the pore volume diminished from 0.93 to 0.61 cm^3 g^{-1}, suggesting a uniform incorporation of sulfur within the ACC substrate. The Al-S battery utilizing this cathode exhibited a high specific capacity of 1320 mAh g^{-1} and a discharge voltage of ≈0.65 V, maintaining a capacity of 1000 mAh g^{-1} after 20 cycles. The microporous structure of the ACC substrate, characterized by pore sizes under 2 nm, enhances electron access, increases the active interfacial area, and reduces the diffusion distance for Al^{3+} ions, effectively improving the solid-phase reaction kinetics of the Al-S battery. Furthermore, Manthiram et al. developed a self-supported composite cathode using carbon nanotubes (CNT) as the conductive substrate. In this design, nanofibers with diameters ranging from 100 to 200 nm interlace to create micrometer-sized pores that accommodate the active sulfur. This cathode exhibits outstanding electrical conductivity, eliminates side reactions associated with binders, and achieves a capacity of 1250 mAh g^{-1} in IL-based Al-S batteries. In a similar vein, a commercially available ordered mesoporous carbon material featuring a hexagonal conductive network (CMK-3) serves as an effective conductive substrate for activated sulfur, achieving a specific capacity exceeding 1500 mAh g^{-1} in Al-S batteries while retaining substantial capacity even after 60 cycles.

Creating porous carbon materials with active sites is a widely used approach to improve reaction kinetics in battery systems.[81–85] Yu et al. synthesized N-doped hierarchical porous carbon (HPCK) with a high specific surface area of 2513 m^2 g^{-1} through a multi-step process.[72] This process included carbonizing a nitrogen-rich polymer precursor, formed by condensing zinc nitrate as a pore-forming agent, followed by etching with KOH. The resulting HPCK material displayed a hierarchical porous structure consisting of macropores, mesopores, and micropores (**Figure 4a**). The macropores facilitate rapid transport of the electrolyte, while the mesopores and micropores effectively house sulfur nanoparticles within a small size range. This hierarchical architecture enhances the electrochemical processes and prevents the cathode structure from collapsing. The nitrogen-doped carbon substrate, known for its superior electrical conductivity, improves charge transfer and aids in the dissociation of chloroaluminate and the reduction of sulfur. This enhancement from nitrogen doping is evidenced by the decreased voltage hysteresis observed in the S/HPCK cathode compared to the Al-S battery with an S/CMK-3 cathode (Figure 4b). The Al-S battery utilizing the S/HPCK cathode achieves a capacity exceeding 1027 mAh g^{-1} at a current density of 0.2 A g^{-1} over 50 cycles, and retains outstanding cycling performance, delivering over 405 mAh g^{-1} after 700 cycles at 1 A g^{-1}.

Ji et al. created a carbonized metal–organic framework material (HKUST-1-C) decorated with copper nanoparticles as a conductive matrix for the sulfur cathode in metal atom catalysis (Figure 4c).[73] The incorporation of Cu nanoparticles not only boosts the electrical conductivity of the porous matrix but also provides catalytic active sites. XRD analysis of the sulfur cathode at different stages (Figure 4d) showed characteristic Cu_xS peaks, suggesting that the copper in the carbon material reacts with polysulfide to form S-Cu ionic clusters. These clusters, characterized by strong interactions and high conductivity, significantly reduce kinetic barriers, enhancing both the efficiency and reversibility of the electrochemical conversion process. The team also explored cobalt ($Co^{II,III}$) as an electrochemical catalyst in combination with the copper nanoparticles.[66] As shown in Figure 4e,f, the introduction of the $Co^{II,III}$ improved polysulfide reactivity and decreased voltage hysteresis. The catalytic influence on sulfur's electrochemical conversion was noticeable whether $Co^{II,III}$ was fixed in the carbon substrate of the positive electrode or dissolved in the IL-based electrolyte. This effect is linked to the formation of cobalt sulfide and the valence changes of $Co^{II,III}$ during charge and discharge cycles. Notably, when the $Co^{II,III}$ was bound in the carbon substrate, the voltage hysteresis measured 0.8 V, reflecting improved reaction kinetics for sulfur conversion in the battery. Furthermore, Yu et al. systematically examined a series of porous carbon-loaded atomic transition metal catalysts (SATM@NC) to assess their catalytic activities in the Al-S battery system (Figure 4g).[74] Both theoretical and experimental results confirmed that stable SATM@NC can significantly enhance the Al-S conversion reactions. Specifically, an Al-S battery incorporating SACo@NC/S maintained a specific capacity of 509.4 mAh g^{-1} after 200 cycles at a current density of 1 A g^{-1}. The distinct roles of nitrogen and oxygen in dual-coordinated single-atom iron catalysts within Al-S batteries were

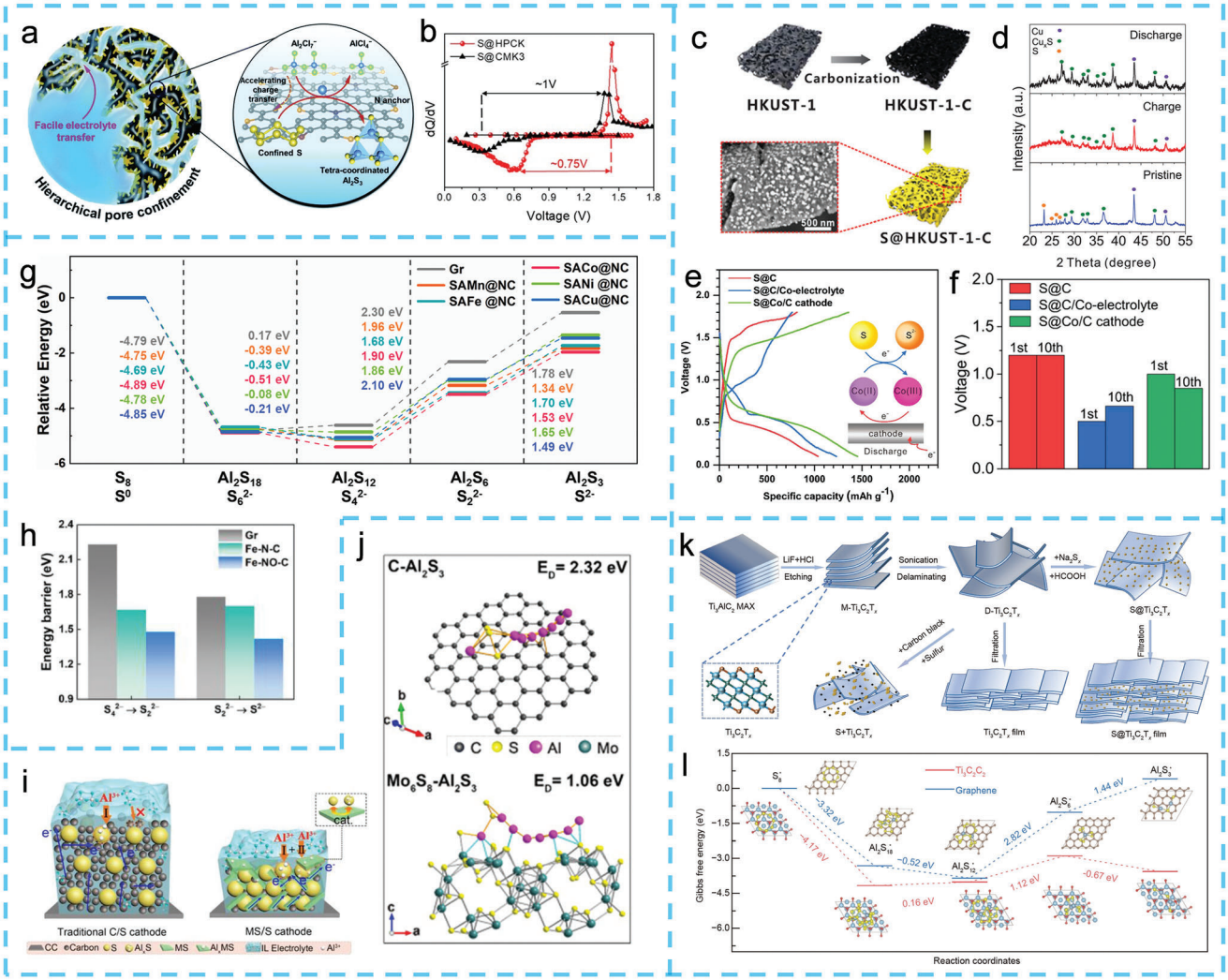

Figure 4. a) Schematic diagram showing the optimization effect and reaction mechanism of the S@HPCK cathode. b) A comparison of the corresponding dQ/dV curves of the charge/discharge curves between the S@HPCK- and S@CMK3-based Al-S batteries at 0.2 A g^{-1}. Reproduced with permission.[72] Copyright 2021, Royal Society of Chemistry. c) S@HKUST-1-C. d) XRD patterns for S@HKUST-1-C cathode in various states. Reproduced with permission.[73] Copyright 2019 John Wiley and Sons. e) Galvanostatic discharge–charge curves measured at a current density of 1 A g^{-1} at 1st cycle and f) their voltage hysteresis at 1st and 10th cycle. Reproduced with permission.[66] Copyright 2020, Wiley-VCH. g) Relative free energy profile for the reduction from S_8 to Al_2S_3 on Gr and SATM@NC. Reproduced with permission.[74] Copyright 2022, Elsevier B.V. h) Comparison of binding energies for Al_2S_3 molecule on Fe–N–C and Fe–NO–C. Reproduced with permission.[75] Copyright 2023, Elsevier. i) The traditional carbon/sulfur cathode and Mo_6S_8/S cathode in Al-S batteries. j) The optimized decomposition pathway of Al_2S_3 on carbon and Mo_6S_8 (101) surfaces. Reproduced with permission.[76] Copyright 2022, Elsevier B.V. k) Schematic of the fabrication of binder-free S@$Ti_3C_2T_x$ film cathodes. l) Gibbs free energy profiles of S_8 and Al_2S_x on monolayer graphene (blue) and $Ti_3C_2O_2$ (red). Reproduced with permission.[77] Copyright 2022, Science China Press and Springer-Verlag GmbH Germany.

also explored. Introducing oxygen lowered the energy barriers to 1.48 and 1.42 eV for Fe—NO—C during crucial rate-determining steps, in contrast to Fe—N—C and graphene (Gr) (Figure 4h).[75] The carefully designed S@Fe—NO—C cathode exhibited excellent cycling stability, maintaining a capacity of 550.1 mAh g^{-1} after 400 cycles and exceptional performance of 352.1 mAh g^{-1} at 3 A g^{-1}, highlighting the significance of advanced single-atom catalyst design for optimizing sulfur cathodes.

In addition to conductive carbon networks, evenly distributing sulfur within alternative conductive matrices, such as Mo_6S_8 and MXene, can also improve reaction kinetics and enhance the electrochemical performance of the battery.[41] Figure 4i shows that the low packing density of traditional carbon materials considerably reduces the energy density of carbon-sulfur composite cathodes. To achieve sufficient electronic conductivity, a significant amount of carbon material is needed, leading to higher electrode porosity and requiring more electrolytes to preserve ionic conductivity. In contrast, using Mo_6S_8 as the conductive network in the cathode, which boasts superior electronic conductivity (138.4 S cm^{-1} compared to 32.3 S cm^{-1} for carbon), allows for faster electron transport, and improves cathode reaction kinetics.[76] Furthermore, density functional theory (DFT)

calculations were conducted to assess the decomposition barriers of Al_2S_3 on both carbon and Mo_6S_8 surfaces. This decomposition process entails the dissociation of an aluminum atom from Al_2S_3 and its diffusion from AlS_3 clusters. The decomposition barrier on Mo_6S_8 is measured at 1.06 eV, which is considerably lower than the 2.32 eV on carbon (Figure 4j), underscoring the effective catalytic role of Mo_6S_8 in the reversible transformation of Al_2S_3. MXene materials, known for their metallic conductivity, adjustable surface chemistry, and plentiful defect sites, serve as effective conductive substrates for sulfur cathodes. Wei et al. developed a binder-free $S@Ti_3C_2T_x$ thin film featuring a sandwich structure for Al-S battery (Figure 4k).[77] This cathode attained a capacity of 489 at 300 mAh g^{-1} and maintained 415 mAh g^{-1} after 280 cycles, achieving an average coulombic efficiency exceeding 95%. Furthermore, DFT calculations suggest that $Ti_3C_2T_x$ can serve as an effective sulfur host, demonstrating stronger binding energy to aluminum polysulfide than graphene. Figure 4l illustrates the Gibbs free energy diagrams for the key reactions of S_8 on monolayer graphene (blue) and $Ti_3C_2O_2$ (red) leading to Al_2S_3 ($S_8 \rightarrow Al_2S_{18} \rightarrow Al_2S_{12} \rightarrow Al_2S_6 \rightarrow Al_2S_3$). The transition from S_8 to Al_2S_3 is hermodynamically favorable, as reflected by a negative Gibbs free energy change, with $Ti_3C_2O_2$ exhibiting a more favorable value of −4.17 eV compared to graphene (−3.32 eV). For $Ti_3C_2O_2$, the conversion of Al_2S_{18} to Al_2S_x (x = 12,6,3) approaches thermodynamic equilibrium, with the peak reaction energy for the conversion from Al_2S_{12} to Al_2S_6 measured at 1.12 eV, which is considerably lower than the 2.82 eV observed for graphene. These theoretical analyses suggest that $Ti_3C_2O_2$ substantially lowers the reaction energy barrier for polysulfide conversion, improves conversion kinetics, and enhances the reversibility of the Al-S battery.

Besides carbon-sulfur composite cathodes and metallic conductive network-based sulfur cathodes, sulfur species are designed to minimize the sulfur conversion reaction pathway. This approach helps prevent the formation of soluble long-chain polysulfides and accelerates reaction kinetics.[88] Among these, polymer sulfur species such as sulfurized polyacrylonitrile (SPAN) are widely utilized in Li-S and Na-S batteries due to their strong covalent bonds and improved ionic-electronic mediation. When polyacrylonitrile is heated with sulfur monomers, it destabilizes its nitrile group, resulting in SPAN, a polymeric material characterized by a pyrrolidine ring structure. This structure contains C═C, C═N, and S—C bonds, which provide high electrochemical reactivity with monovalent cations and allow for electronic conductivity of up to 10^4 S cm^{-1}. Ming et al. utilized SPAN as a cathode material in the Al-S battery system, employing ex situ electron paramagnetic resonance spectroscopy (EPR) to investigate the relationship between polymer molecular structure and electrochemical mechanisms.[86] This approach aimed to elucidate the electrochemical behavior in the organic polymer-sulfur system and the free radical mechanism proposed for the Li-SPAN battery system. As shown in **Figure 5a**, sulfur radical signals appear and increase in intensity from the pristine SPAN to the $1D_{400}$ discharge state, which is attributed to the progressive cleavage of S—S bonds and the formation of sulfur radicals in the presence of Li^+ during discharge. Further discharging to the 1Dtotal state results in a decrease in sulfur radical intensity, indicating that the radicals chemically bind with Li^+ following electron coupling, highlighting the redox reaction between sulfur/nitrogen in SPAN and lithium ions. Upon charging the battery back to $1C_{total}$, the sulfur radical signal increased, indicating the extraction of Li^+ from the SPAN structure and the regeneration of the sulfur radical. During further charging, the sulfur radicals remained stable. The electron transfer process in SPAN can be clarified by modeling the steric configurations of radical and ionic SPANs, as shown in Figure 5b, which illustrates the potential evolution of the SPAN structure. Initially, the cleavage of S—S bonds in pristine SPAN produces a linear radical SPAN, which easily transitions to a conjugated π structure, stabilizing the sulfur group. Simultaneously, when SPAN receives electrons from the external circuit, the radical SPAN converts to ionic SPAN, while electrostatic repulsion alters the linear structure to a "zigzag" configuration. The molecular structure's ample space and numerous negative sites make it highly reactive with lithium, facilitating the generation of free radical SPAN from pristine SPAN through reduction. This mechanism led to further examination of the SPAN cathode's reactivity with Al^{3+} ions.

Cyclic voltammograms (Figure 5c) show an activation plateau at 0.3 V (versus Al/Al^{3+}) during the initial cycle, linked to the cleavage of S—S bonds, which corresponds to an increase in discharge capacity from 320 to 605 mAh g^{-1} (Figure 5d). The conjugated structure containing sulfur radicals in SPAN improves reaction kinetics. However, the slow conversion of aluminum polysulfide to sulfur leads to the persistence of insulating sulfur between the collector and polysulfide, even after complete discharge. This situation hinders electron and ion transfer during charge and discharge cycles, ultimately degrading reaction kinetics and reversibility. Ji et al. have shown that in Al-S batteries, the electrochemical reaction is localized to the sulfur cathode when Al_2S_3 is used as the cathode material, proving to be more efficient than traditional sulfur cathodes.[87] Al_2S_3 enables a rapid solid-liquid conversion reaction with aluminum polysulfide, effectively preventing the formation of S_0. This leads to improved reaction reversibility, enhanced coulombic efficiency, and better reaction kinetics (Figure 5e). Furthermore, UV–vis spectroscopy of the electrolyte-impregnated diaphragm indicated that the main oxidation product of Al_2S_3 during charging is S_6^{2-}, which may also serve as the final oxidation product (Figure 5f).

3.2. Electrolyte Design

In addition to cathode design to enhance reaction kinetics, the development and selection of a suitable electrolyte are essential for achieving high-performance Al-S batteries. Compared to lithium-sulfur batteries, the electrolyte systems for Al-S batteries are less developed due to limited research time. Currently, these electrolytes can be classified into several categories: 1) conventional ionic liquid electrolytes,[38,54] 2) ionic liquid analog electrolytes,[61,62] 3) inorganic molten salt electrolytes,[40,68,89] 4) quasi-solid electrolytes,[90] and 5) aqueous electrolytes.[52,53,63,91,92]

3.2.1. Ionic Liquid Optimization

Ionic liquids, comprising organic cations and inorganic or organic anions, have been extensively utilized in non-aqueous

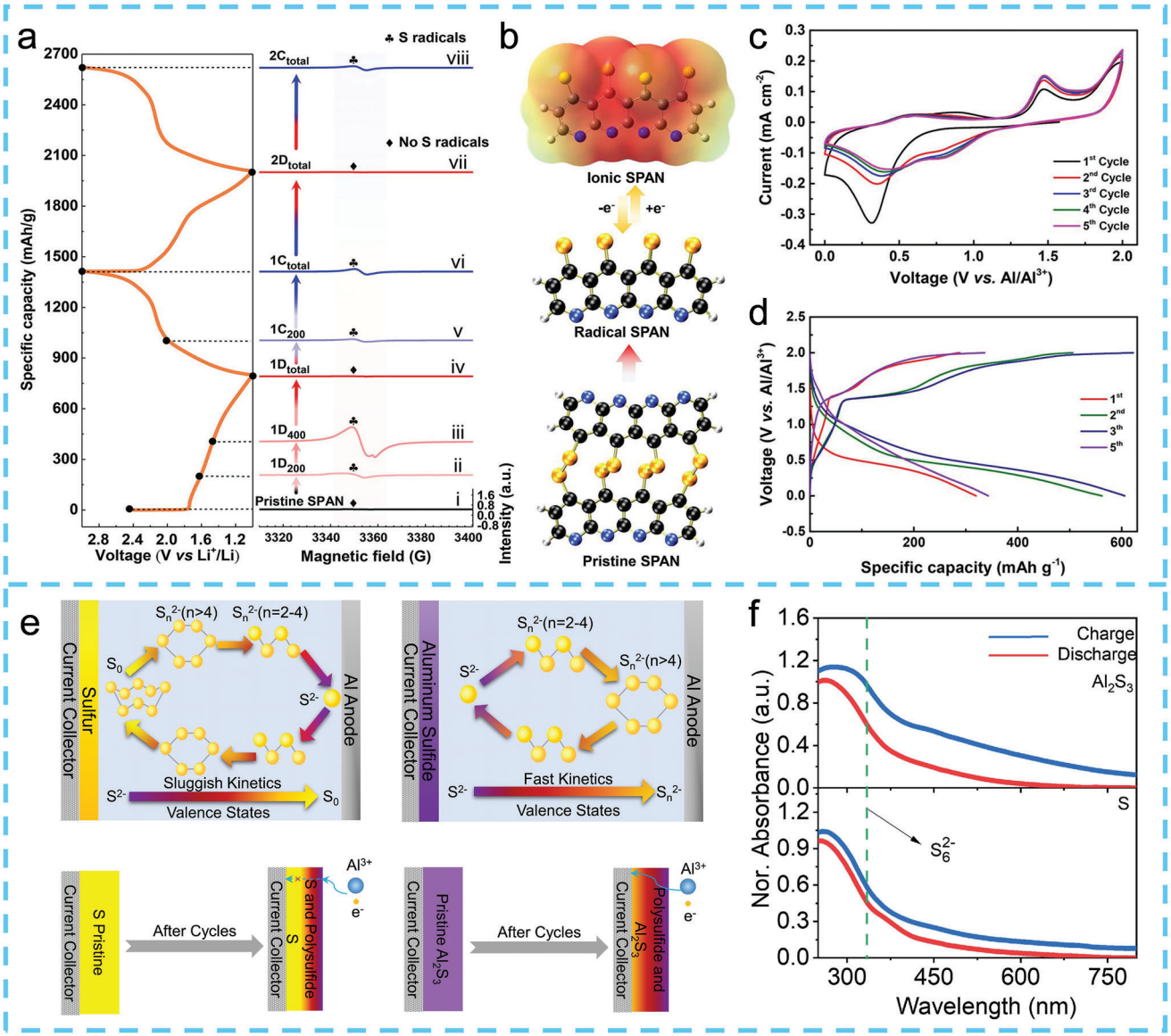

Figure 5. a) Galvanostatic (dis-)charge curves of SPAN in the first and second cycles and the corresponding ex situ EPR spectra. b) Proposed structural evolution from pristine SPAN to the intermediates of radical and ionic SPAN in the reactions. c) Cyclic voltammograms and d) galvanostatic (dis-)charge curve of SPAN in Al–S battery applications. Reproduced with permission.[86] Copyright 2018 American Chemical Society. e) The illustration of the process of sulfur species conversion in S and Al_2S_3 cathode. f) UV–vis spectra of the electrolyte after 5 discharge–charge cycles in the Al-S battery assembled with S and Al_2S_3 cathodes. Reproduced with permission.[87] Copyright 2021 Wiley-VCH GmbH.

aluminum-based batteries to enhance interfacial properties and achieve highly reversible aluminum metal stripping and plating. Recently, room-temperature ILs have been suggested as electrolytes for Al-S batteries due to their excellent ionic conductivity, thermal stability, low flammability, and minimal side reactions, presenting a promising avenue for developing rechargeable Al-S batteries.

Since the introduction of room-temperature ILs, specifically those containing $AlCl_3$ and chlorinated 1-methyl-3-ethylimidazole, in aluminum-sulfur (Al-S) batteries in 2015, Wang et al. have successfully created the first rechargeable Al-S battery utilizing ILs as the electrolyte, reaching an energy density of 650 Wh kg^{-1}. In this battery system, sulfur experiences a solid-state conversion reaction, while higher temperatures help minimize voltage hysteresis. Researchers have implemented several optimization strategies to improve the properties of IL electrolytes. Li et al. substituted $Al_2Cl_7^-$ with $AlCl_6Br^-$ in the IL system, which lowered the dissociation energy barrier for long-chain chloroaluminate.[57] Based on the Arrhenius equation, this modification enhanced the dissociation reaction rate by a factor of 15, thereby significantly improving the reaction kinetics of the Al-S battery (**Figure 6**a,b). Consequently, a reversible Al-S battery was achieved with up to 82% sulfur utilization using the NBMPBr/$AlCl_3$ electrolyte, which exhibited excellent electrochemical stability. As shown in Figure 6c, the Al-S battery employing the EMICl/$AlCl_3$ electrolyte displays minimal discharge

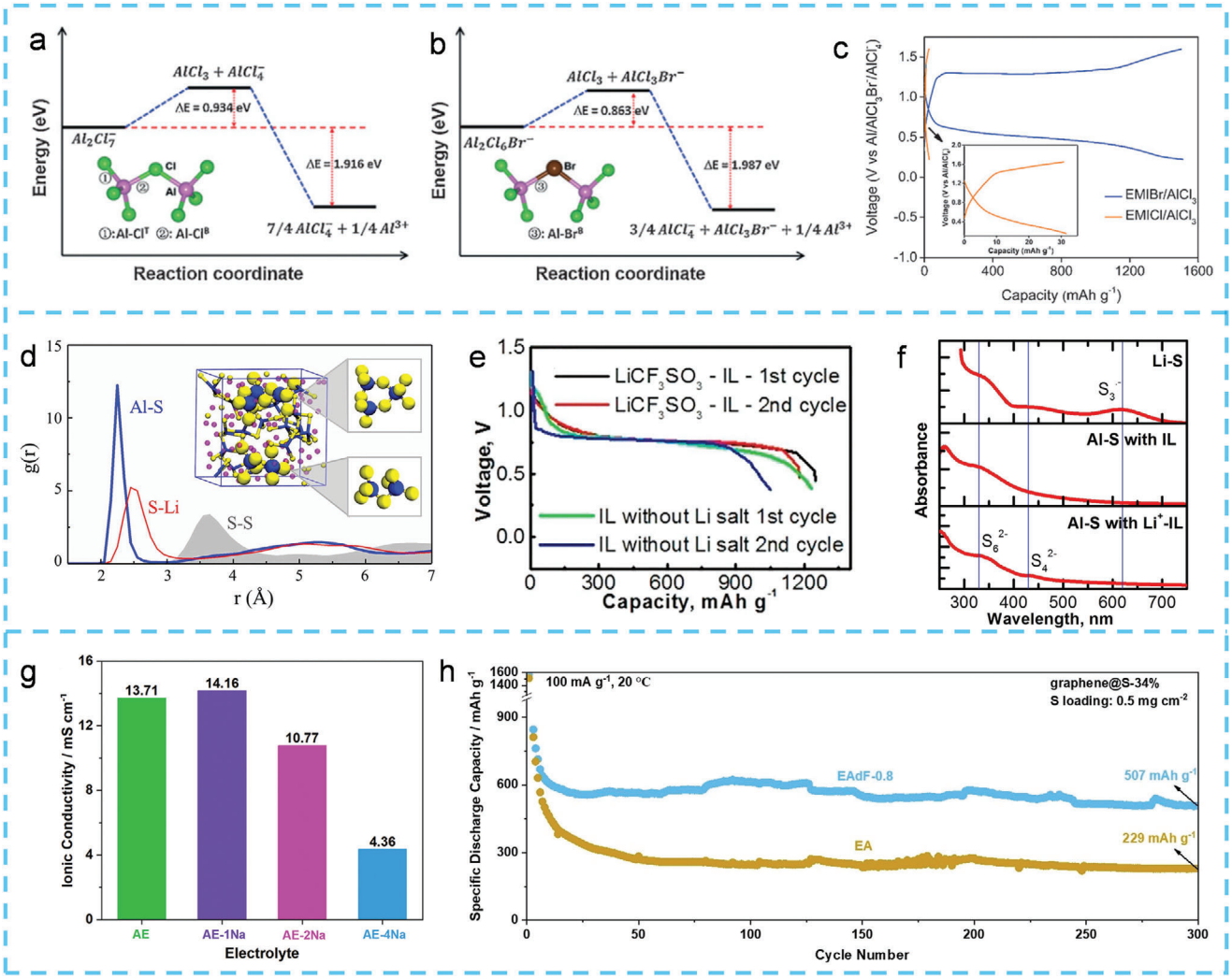

Figure 6. a,b) Energy profiles of the dissociation reactions with $Al_2Cl_7^-$ and $Al_2Cl_6Br^-$ electrolytes. c) Charge/discharge profile with the EMIBr/$AlCl_3$ or EMICl/$AlCl_3$ (inset) electrolytes at 251 mA g^{-1}. Reproduced with permission.[57] Copyright 2018, Wiley-VCH GmbH. d) Radial distribution functions for S–S, Li–S, and Al–S pairs as predicted from ab initio molecular dynamic simulations. e) First and second discharge profiles with the ionic liquid or Lithium-Ion-Mediated ionic liquid electrolytes. f) UV–vis spectra of the sulfur cathodes discharged to a depth of 350 mA h g^{-1} with different ionic liquids. Reproduced with permission.[58] Copyright 2017, Elsevier. g) Ionic conductivity of the $[AlCl_3]_{1.3}[EmimCl]_1$ and NaCl-containing electrolytes. Reproduced with permission.[93] Copyright 2023 The Authors. Advanced Functional Materials published by Wiley-VCH GmbH. h) Evolution of discharge-specific capacity upon long-term dis-/charge cycling at the current density of 100 mA g^{-1} with EA and EAdF-0.8 electrolytes at 20 °C. Reproduced with permission.[60] Copyright 2024 The Authors. Angewandte Chemie published by Wiley-VCH GmbH.

capacity in comparison to its counterpart with the same S@CMK-3 cathode. In contrast, the battery utilizing the EMIBr/$AlCl_3$ electrolyte displays considerably reduced polarization and achieves an initial discharge capacity of 1500 mAh g^{-1} at a current rate of 251 mA g^{-1}. Likewise, Manthiram et al. found that an IL electrolyte incorporating lithium salt additives improves the reversibility of aluminum polysulfides, resulting in a mixture of Li_2S and Al_2S_3 at the discharge stage (Figure 6d).[58] Figure 6e illustrates the discharge mechanism of Al-S batteries, where the high-voltage discharge region, marked by slopes or plateaus, is generally associated with the transformation of elemental sulfur into soluble higher-order polysulfides. Notably, in the absence of lithium salt in the electrolyte, the high-voltage plateau disappeared by the second cycle. In contrast, the lithium-ion-mediated IL exhibited no notable difference in discharge curves between the two cycles. UV–vis spectroscopy analysis of the sulfur discharge state cathode, conducted before and after introducing the modified electrolyte (Figure 6f), reveals substantial differences. With the modified electrolyte, two distinct absorption peaks at 330 and 430 nm are observed, indicating the presence of soluble S_6^{2-} and S_4^{2-} species. This observation confirms that elemental sulfur dissociates into these soluble species at the expected discharge depth. Conversely, the unmodified electrolyte shows only a single peak at 330 nm, indicating the presence of soluble S_6^{2-} species, while S_4^{2-} species remain insoluble in the IL electrolyte. These UV–vis results suggest that Li^+ ions enhance the solubility of S_4^{2-} species. Electrochemical characterizations indicate that lithium-ion mediation increases the solubility of

polysulfides in the electrolyte, significantly enhancing the kinetics and reversibility of the reaction.

Recently, Passerini et al. have explored various additive-based modifications to conventional IL electrolytes, yielding relatively favorable outcomes. Figure 6g illustrates that incorporating 1 and 2 wt.% of alkali metal chlorides (LiCl, NaCl, KCl) into the IL electrolyte enhances ionic conductivity and optimizes the dynamic equilibrium between $Al_2Cl_7^-$ and $AlCl_4^-$, leading to significantly better cycling performance of Al-S batteries compared to conventional electrolytes. Additionally, a locally concentrated IL electrolyte (LCILE) has been proposed, formed by diluting the IL with a non-solventized 1,2-difluorobenzene cosolvent. This approach aims to improve mobility and ionic conductivity without disturbing the $AlCl_4^-/Al_2Cl_7^-$ equilibrium.[60] This preserves the reversible aluminum stripping and plating processes while accelerating reaction kinetics in Al-S batteries. Notably, at 20 °C, the Al-S battery with LCILE maintained a capacity of 507 mAh g^{-1} after 300 cycles, while the capacity with a dFBn-free electrolyte was only 229 mAh g^{-1} (Figure 6h).

3.2.2. Ionic Liquid Analog Electrolytes

The development of low-cost IL electrolytes presents a promising strategy for enhancing the performance of Al-S batteries. Notably, Lin et al. reported a urea-based $AlCl_3$-Urea electrolyte that exhibits highly reversible operation of Al-S batteries. This electrolyte facilitates a high discharge voltage plateau of ≈1.6–2.0 V with an initial capacity of 740 mAh g^{-1}.[61] Importantly, the chemical stabilization of sulfur within this electrolyte allows for a capacity retention of 85.3% after 100 cycles, in contrast to the instability observed in conventional battery systems (**Figure 7a**). Yu et al. developed a cost-effective $AlCl_3$/acetamide deep eutectic solvent electrolyte for Al-S batteries, achieving an initial capacity exceeding 1500 mAh g^{-1} and maintaining 500 mAh g^{-1} after 60 cycles, demonstrating commendable performance (Figure 7b).[62] Spectroscopic analysis identified the presence of $AlCl_4^-$, $Al_2Cl_7^-$, and $[AlCl_2\cdot(AcA)_2]^+$ ions as contributing factors. Furthermore, the kinetics of the battery's conversion reaction in this electrolyte can be improved through the use of various additives. As depicted in Figure 7c, a locally concentrated deep eutectic liquid electrolyte was developed by adding non-solvated 1,2-difluorobenzene to a urea-based IL electrolyte.[94] The addition of 1,2-difluorobenzene significantly enhanced ionic mobility and transport without compromising ionic kinetics. The Al-S battery featuring the modified electrolyte exhibited significant capacity improvement and enhanced reaction kinetics compared to the unmodified version after 20 cycles at 0.1 A g^{-1} (Figure 7d). Additionally, the introduction of 1,2-difluorobenzene modified the solid-electrolyte interface on the aluminum anode, leading to reduced interfacial resistance. The lifespan of the aluminum/aluminum battery increased from 210 to 2000 h, while polarization decreased from 0.36 to 0.14 V at a current density of 1.0 mA cm^{-2} (Figure 7e). Araez et al. demonstrated, as depicted in Figure 7f, that adding NaI or LiI as electrolyte additives to urea-based ILs significantly reduced the charging voltage plateau of the Al-S battery by ≈0.23 V.[59] This addition improved the battery's kinetics and catalyzed the electrochemical reaction process. The redox mediator provides an alternative pathway for the electrochemical reaction, allowing for its reversible oxidation and reduction, thus preventing its depletion. This phenomenon can be explained by two reactions that take place during the charging of Al_2S_3:

$$9I^- \rightarrow 3I_3^- + 6e^- \quad (5)$$

$$Al_2S_3 + 3I_3^- \rightarrow 3/8S_8 + 2Al^{3+} + 9I^- \quad (6)$$

When NaI or LiI redox mediators are introduced, Al_2S_3 experiences chemical oxidation through its reaction with triiodide (I_3^-) (Figure 7g), rather than undergoing electrochemical oxidation. Conversely, in the absence of a dielectric, Al_2S_3 must transfer electrons to the collector through a conductive carbon network, which demonstrates poor reaction kinetics. In the realm of AcA-based IL electrolytes, Yu et al. investigated several fluorine-substituted AcAs as potential additives. Electrochemical analyses revealed that the dFAcA-modified $AlCl_3$/AcA electrolyte improved the kinetics and stability of the deposition and stripping reactions of aluminum electrodes. X-ray photoelectron spectroscopy (XPS) analyses indicated that dFAcA promoted the formation of AlF_x on aluminum electrodes during these processes, stabilizing the electrode, reducing interfacial resistance, and enhancing reaction kinetics.

3.3. Molten Salt Electrolyte

The electrochemical behavior of sulfur and sulfides in molten salts has been studied over the past century. Recently, our group developed fast-charging molten salt Al-S batteries that are notable for their high safety and low cost.[40] **Figure 8a** shows the solvation structure surrounding Al^{3+} and its desolvation energy, analyzed through ab initio molecular dynamics (AIMD) simulations of two electrolytes: EMIC-$AlCl_3$ IL and NaCl-$AlCl_3$ molten salt. In both cases, Al^{3+} typically forms tetrahedral coordination with Cl^-, resulting in the formation of $AlCl_4^-$ and $Al_2Cl_7^-$ clusters. A notable difference is the formation of higher-order $Al_3Cl_{10}^-$ in the NaCl-$AlCl_3$ melt, with AIMD trajectories also revealing transient $Al_4Cl_{13}^-$ species (Figure 8a,b). Unlike the larger EMI^+ cations present in the EMIC-$AlCl_3$ IL, Na^+ facilitates the migration of Cl^-, thereby improving the kinetics of the battery reactions. The electrochemical process was demonstrated with a sulfur-graphene composite, where sulfur maintained a stable voltage-time profile averaging 1.05 V, with an initial capacity of 1350 mAh g^{-1} at C/5. Notably, the polarization voltage was as low as 50 mV, in contrast with the higher polarization voltages observed in EMIC-$AlCl_3$ electrolytes: 450 mV (C/20) at 25 °C and 60 °C, 250 mV (C/20) at 25 °C and 60 °C, and 205 mV (C/5) at 110 °C. Furthermore, the Al-S battery using EMIC-$AlCl_3$ displayed a significant overcharge plateau and low sulfur utilization across all temperatures, indicating considerable dissolution of intermediates in the electrolyte (Figure 8c). At a constant discharge rate of C/2, the Al-S battery achieved a capacity of 500 mAh g^{-1} at a charging rate of 10 C, which slightly decreased to 430 mAh g^{-1} at 20 C and 360 mAh g^{-1} at 50 C. Even at elevated charge rates of 100 and 200 C (335 A g^{-1} and 670 mA cm^{-2}), the batteries have maintained capacities of 280 and 210 mAh g^{-1}, respectively. In contrast, the capacity of the battery using EMIC-$AlCl_3$ was close to zero at this temperature and charging rate (Figure 8d).

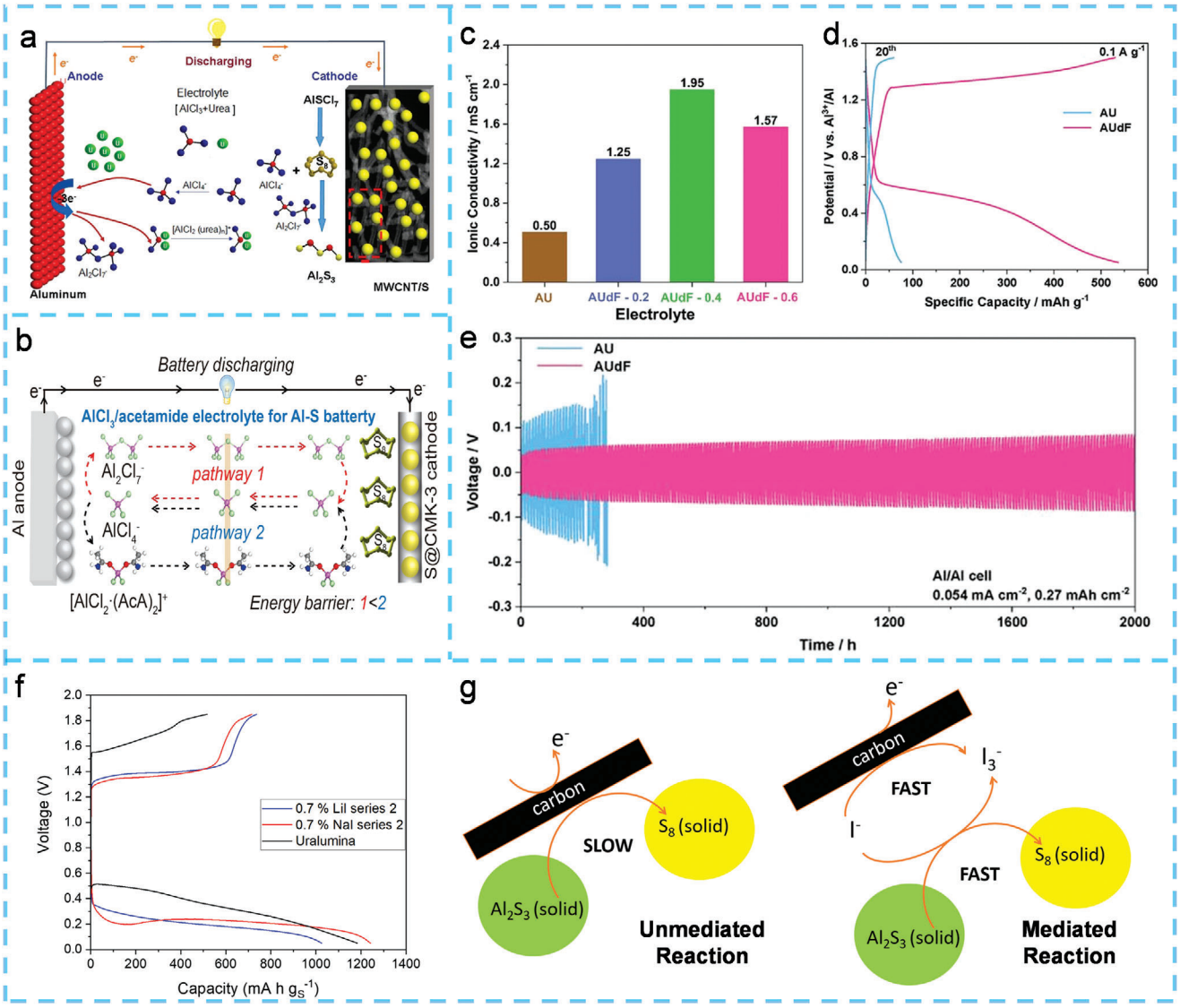

Figure 7. a) Schematic representation of the urea-supported Al–S batteries. Reproduced with permission.[61] Copyright 2018, Wiley-VCH GmbH. b) Schematic illustration of the battery discharging process with the corresponding energy profiles standing for AcA coordinated with $AlCl_2^+$ through different sites (where Cl: green; O: red; Al: pink; C: gray; H: white; N: blue). Reproduced with permission.[62] Copyright 2019, Elsevier. c) Ionic conductivity of $[AlCl_3]_{1.3}[Urea]_1$ and AUdF-x at 20 °C. d) Evolution of specific discharge capacity upon cycling at 0.1 A g^{-1}.e) Voltage evolution upon long-term stripping/plating cycles (5 h for each step) at 0.054 mA cm^{-2} of Al/Al symmetric cells employing AU and AUdF-0.4 as electrolytes at 20 °C. Reproduced with permission.[94] Copyright 2024 The Authors. Advanced Materials published by Wiley-VCH GmbH. f) Comparison of charging and discharging voltage platform of urea electrolyte before and after introduction of iodide mediator (LiI, NaI) at small concentration (0.7 wt%). g) Proposed mechanism of non-mediated and mediated (with iodide) charging reactions of Al-S batteries. Reproduced with permission.[59] Copyright 2021 The Authors. ChemSusChem published by Wiley-VCH GmbH.

Our group demonstrated a rapid-charging Al-S battery by adjusting the electrolyte component ratios, employing an entropy-enhancing quaternary chloroaluminate electrolyte at 85 °C, just below the boiling point of water.[68] This study presents a quaternary alkali metal chloroaluminate melt composed of $AlCl_3$, NaCl, LiCl, and KCl, which has a melting point ≈80 °C lower than that of binary and ternary molten salt systems (Figure 8e). In this melt, $AlCl_3$ acts as a Lewis acid, while the alkali metal chlorides serve as Lewis bases. Deviations from the eutectic salt ratio raise the melting points, underscoring the considerable influence of the salt ratio on the electrolyte's physical properties—such as melting point, viscosity, and ionic conductivity—which subsequently affect the battery's electrochemical performance. In molten salts, the latent heat of fusion determines the energy required to overcome the electrostatic attraction between cations and anions; weaker attractions lead to lower melting temperatures (Figure 8f). The quaternary molten salt electrolyte, rich in electrochemically active higher-order Al-Cl clusters, demonstrates a low melting point conducive to the rapid desolvation of Al^{3+}. As depicted in Figure 8g, the molten salt Al-S battery retains 85.4% of its capacity after 1400 cycles at a charge rate of 1 C at 85 °C. Importantly, the asymmetric sulfur reaction

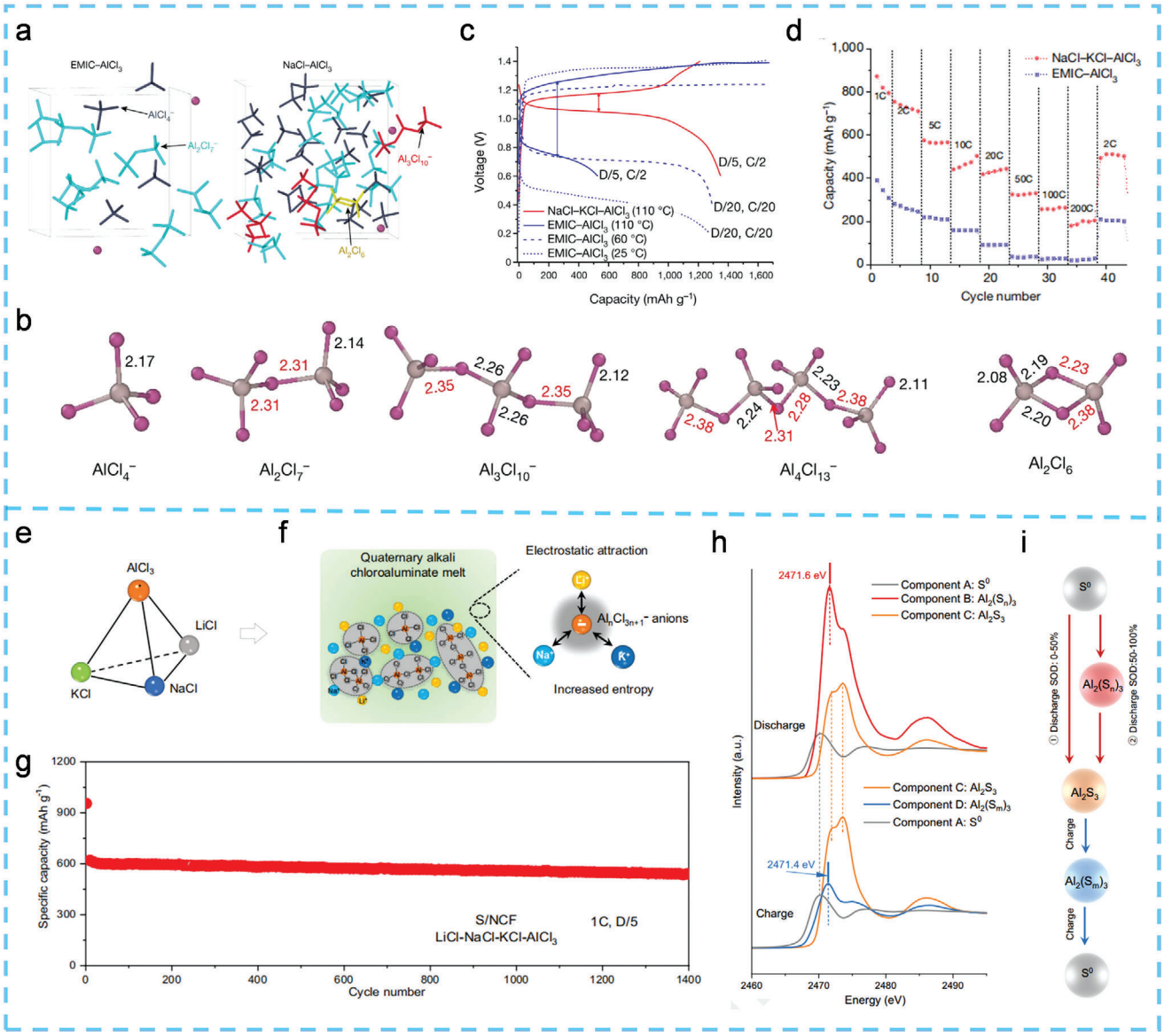

Figure 8. a) Typical snapshots from the AIMD trajectories showing the different chloroaluminate solvation clusters for the EMIC-$AlCl_3$ and NaCl-$AlCl_3$ electrolytes. b) The representative configuration of the clusters taken from the calculated equilibrium states; the Al and Cl atoms are shown in grey and purple, respectively, and the numbers represent the Al–Cl bond length in ångströms, with red values indicating a relatively longer distance. c) Typical voltage–capacity traces of Al|NaCl–KCl–$AlCl_3$|S cells at different temperatures. d) The charge rate performance of Al|NaCl–KCl–$AlCl_3$ |S cells at different charging rates and constant discharging rate (D/2) at 110 °C. Reproduced with permission.[40] Copyright 2022 Springer Nature Limited. e) Tetrahedral diagram of the four components for inorganic molten salt electrolyte, showing the basis for the phase diagram for the electrolyte formulations. f) Design principles for the quaternary alkali melt electrolyte, showing the presence of a high-order $Al_nCl_{3n+1}^-$ cluster that has a more delocalized charge density. g) Long-term cycling performance of the S/NCF composite cathode at a discharging rate of D/5 and a high charging rate of 1 C at 85 °C. h) S K-edge XANES spectra of the three identified primary components during discharge, including S^0 (A, black), $Al_2(S_n)_3$ (B, red), and Al_2S_3 (C, orange), and the three during charge, including S_0 (A, black), $Al_2(S_m)_3$ (D, blue) and Al_2S_3 (C, orange). i) Schematic illustration of the proposed asymmetric reaction pathways of the molten salt Al–S battery. Reproduced with permission.[68] Copyright 2024 The Author(s).

mechanism, which involves polysulfide intermediates, was clarified using in situ synchrotron near-edge absorption spectroscopy, among other analytical techniques (Figure 8h,i). During the discharge state (SOD) of 0–50%, S^0 is directly converted to Al_2S_3 without the formation of $Al_2(S_n)_3$, indicating a two-phase reaction process (Equation 8). The dynamics of S° conversion appear unusually low at this stage, likely due to the dynamic reduction in sulfur particle size during discharge and the variable sulfur self-adsorption effect. Upon further discharge, $Al_2(S_n)_3$ forms, suggesting that residual S^0 undergoes a three-phase transition (S^0-$Al_2(S_n)_3$-Al_2S_3) as described in Equations 9 and 10. Figure 8i illustrates that S° follows two reaction pathways that lead to the final Al_2S_3 product at different discharge stages. During charging, Al_2S_3 undergoes a multiphase transformation

(Al_2S_3-$Al_2(S_m)_3$-S^0), which is distinct from the discharge process (Equations 11 and 12; Figure 8i). This result demonstrates that the formation of $Al_2(S_m)_3$ intermediates during charging is vital for rapid charging of Al-S batteries at 85 °C. Notably, the desolvation of Al^{3+} from the chloroaluminate electrolyte occurs before any reaction takes place (Equation 7).

The Al^{3+} desolvation:

$$4Al_nCl_{3n+1}^- \rightarrow (n-1)\,Al^{3+} + (3n+1)\,AlCl_4^- \quad (7)$$

Reaction on discharge:

$$3S^0 + 2Al^{3+} + 6e^- \rightarrow Al_2S_3 \quad (8)$$

$$3nS^0 + 2Al^{3+} + 6e^- \rightarrow Al_2(S_n)_3 \quad (9)$$

$$Al_2(S_n)_3 + 2(n-1)\,Al^{3+} + 6(n-1)\,e^- \rightarrow nAl_2S_3 \quad (10)$$

Reaction on charging:

$$mAl_2S_3 - 6(m-1)\,e^- \rightarrow Al_2(S_m)_3 + 2(m-1)\,Al^{3+} \quad (11)$$

$$Al_2(S_m)_3 - 6e^- \rightarrow 3mS^0 + 2Al^{3+} \quad (12)$$

3.4. Kinetic Promotion Strategy Based on Sulfur Oxidation Reaction

In contrast to traditional Al-S batteries that depend on sulfur reduction (where elemental sulfur is reduced to S^{2-} and oxidized back to S^0), some researchers have suggested a mechanism centered around sulfur oxidation. Experiments indicate that sulfur can be reversibly oxidized to S^{4+} in a urea-based IL electrolyte when the maximum charging voltage of the Al-S battery is increased to 2.4 V relative to Al^{3+}/Al. Theoretically, this mechanism can yield a capacity of up to 3350 mAh g^{-1} during the S/S^{4+} redox cycle.[95] Qiao et al. revealed that sulfur oxidation involves the intermediate SCl_3^+, which forms $SCl_3{\cdot}AlCl_4$ (**Figure 9a**) and can be reduced back to sulfur at ≈1.8 V.[39] As illustrated in Figure 9b, the sulfur oxidation process exhibits a high discharge voltage plateau near 1.8 V, while the reduction process shows a significantly lower discharge voltage of ≈0.5 V. During sulfur oxidation (Figure 9c), the peaks corresponding to the (102), (013), and (110) facets of $AlSCl_7$ sequentially emerge as the Al-S battery charges to 2.4 V. When reverting from $AlSCl_7$ back to sulfur, these peaks disappear, leaving only the characteristic peak of sulfur. Notably, the diffraction peak at 10.8°, indicative of sulfur, remains present throughout the charging and discharging cycles, indicating incomplete electrochemical oxidation. This evidence confirms the efficient oxidation of sulfur to $AlSCl_7$ and the reversible transition between $AlSCl_7$ and sulfur. In the sulfur reduction process (Figure 9d), Al_2S_3 exhibits diffraction peaks at 8.5° and 16.6°, corresponding to (011) and (016) facets, respectively. These peaks diminish during reverse charging as Al_2S_3 reverts back to sulfur. However, the characteristic peaks at (100) and (016) for Al_2S_3 are observed during charging, indicating the difficulty of the reversible decomposition of Al_2S_3 into sulfur. As depicted in Figure 9e, Raman spectral peaks at ≈145, 210, and 462 cm^{-1} are associated with sulfur. The intensity of these peaks decreases during charging, signifying the conversion of sulfur to $AlSCl_7$. During reverse discharge, the reappearance of these sulfur peaks strongly indicates the high reversibility of sulfur oxidation. Notably, a new peak emerges at 530 cm^{-1}, attributed to vibrations associated with the SCl_3^+ cation. To assess the sulfur valence state during oxidation, XPS measurements were conducted at various oxidation voltages (Figure 9f). The S 2p XPS spectra display peaks at ≈169.4 and 168.3 eV, positioned between the +2 and +6 thiosulfate states, which gradually appear and are attributed to +4 sulfur, confirming the stable presence of $AlSCl_7$ oxidation products. The specific reaction process of this Al-S battery based on sulfur oxidation reaction can be described as Equation 13:

$$S + 7AlCl_4^- \leftrightarrow SCl_3AlCl_4 + 3Al_2Cl_7^- + 4e^- \quad (13)$$

In addition, Yu et al. developed an Al-S battery utilizing AcA-based ILs, achieving a discharge voltage of ≈1.8 V.[65,95] To evaluate the electrochemical properties of sulfur for battery design, theoretical calculations were performed on sulfur reduction products tetra-Al_2S_3(s), pristine S_8(s), and oxidation products, including S_2Cl_2(l), SCl_2(l), SCl_4(l) and $SCl_3{\bullet}AlCl_4$. Density functional theory (DFT) was used to optimize the molecular models of these compounds, as depicted in Figure 9g. Theoretical potentials for S_8, S_2Cl_2, SCl_2, and SCl_4, representing typical S^0, S^{1+}, S^{2+}, and S^{4+} states, were calculated to be 1.25, 1.84, 2.03, and 2.10 V versus Al^{3+}/Al, respectively. Notably, the theoretical potentials of S_2Cl_2 、 SCl_2, and SCl_4 fall within the electrochemical window of the $AlCl_3$/AcA electrolyte, indicating that reversible electrochemical oxidation of sulfur can be activated in $AlCl_3$/AcA-based Al-S batteries at elevated voltages. As shown in Figure 9h, the reversible oxidation reaction of sulfur, which has a voltage polarization of ≈0.55 V, displays lower electrode polarization compared to the reversible reduction reaction of sulfur, which has a polarization of ≈1.2 V. This results in enhanced reaction kinetics and energy efficiency compared to Al-S batteries that rely on sulfur reduction. This enhancement may be attributed to improved interfacial contact facilitated by the liquid medium and the single-electron-transfer oxidation of sulfur. The discharge curve reveals two voltage plateaus at ≈1.91 and 1.75 V (Figure 9h). Furthermore, batteries using commercial S_2Cl_2 as the cathode material display similar discharge voltage plateaus (Figure 9i), indicating these plateaus likely result from the stepwise reduction of S_2Cl_2. Notably, in contrast to conventional Al-S batteries, high-voltage Al-S batteries do not produce polysulfides during the reaction, resulting in enhanced capacity retention and improved electrochemical conversion kinetics.

4. Shuttle Suppression Strategies

Since the significant advancement in Al-S battery technology in 2015, researchers have focused extensively on enhancing the electrochemical performance of these batteries. Despite progress in the practical application of Al-S systems, electrochemical tests have identified several issues, including poor cycle stability and relatively low utilization of active materials. To address these issues, various verification experiments and characterizations have been conducted. Similar to other metal-sulfur batteries, the dissolution of polysulfide intermediates during sulfur reduction is a primary cause of these

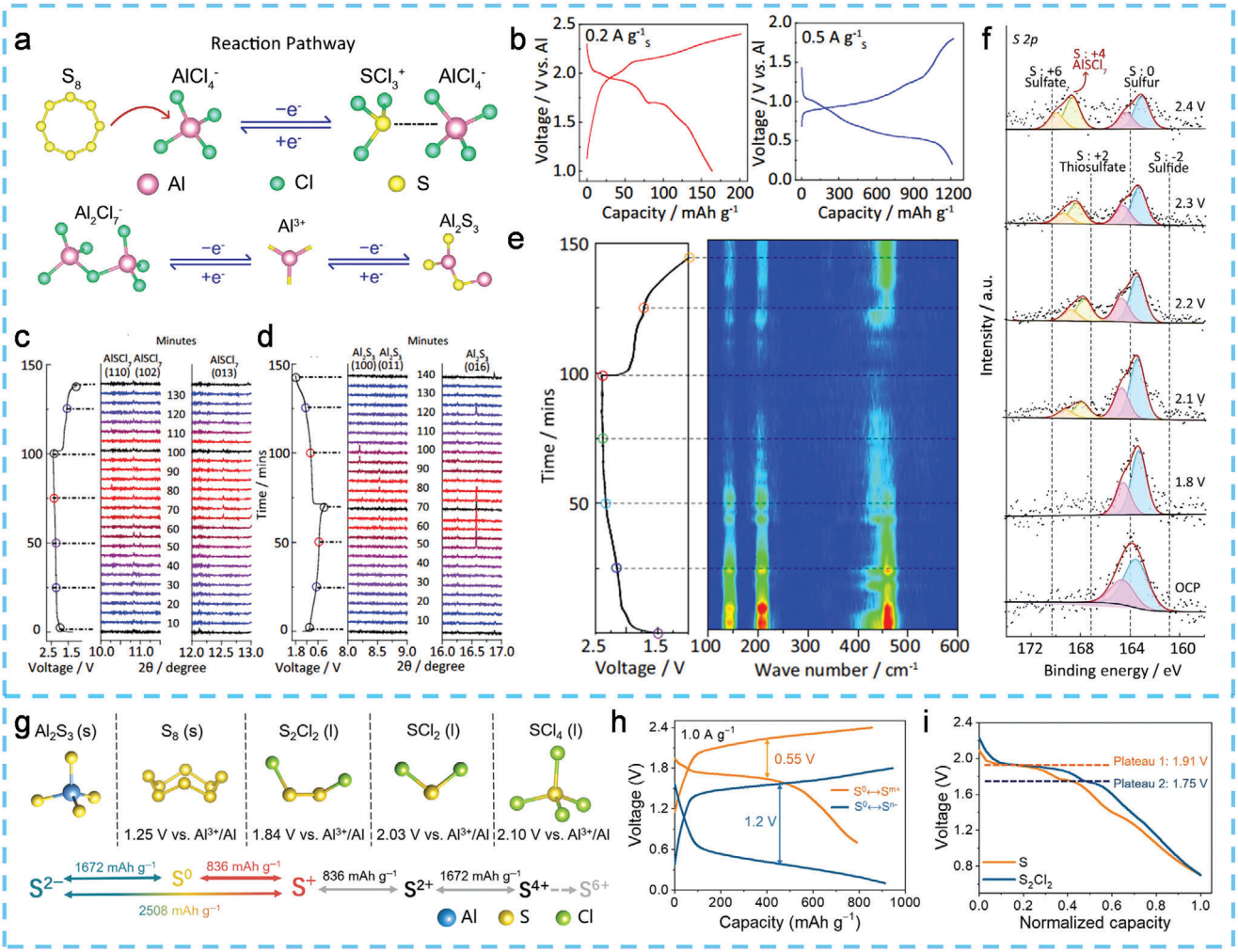

Figure 9. a) Schematics for sulfur oxidation and sulfur reduction processes with $AlCl_4^-$ and $Al_2Cl_7^-$ anions, respectively. b) Galvanostatic charge–discharge curves of the S/CNT cathode based on e sulfur oxidation at 0.2 A g^{-1} and sulfur reduction at 0.5 A g^{-1}.The time-dependent in situ synchrotron-based XRD patterns for c) sulfur oxidation and d) sulfur reduction processes and the corresponding charge–discharge curves. The current densities for sulfur oxidation and sulfur reduction are 0.2 and 0.5 A g^{-1}, respectively. e) The charge–discharge curves of Al–S batteries at 0.2 A g^{-1} and their real-time Raman contour map for S/CNT cathode. f) Ex situ S 2p XPS spectra of S/CNT cathode at different oxidation voltages. Reproduced with permission.[39] Copyright 2023 Wiley-VCH GmbH. g) Based on the theoretical calculation of the potential of different S species and Al^{3+}/Al in the electrochemical oxidation of sulfur. h) A comparison between representative voltage profiles of Al-S batteries based on the reversible oxidation and reversible reduction of S at a current density of 1.0 A g^{-1}. i) The normalized discharge curves of S and S_2Cl_2 as active cathode materials in Al-S batteries. Reproduced with permission.[65] Copyright 2022 Wiley-VCH GmbH.

challenges.[69,96] The inherent properties of ILs enable the soluble high-order AlPSs generated during discharge to dissolve readily in the electrolyte, significantly diminishing the reversibility of the active material reactions within the battery system. Furthermore, dissolved AlPSs can migrate through the separator and accumulate on the aluminum anode, creating a "dead sulfur" issue that is non-reusable and substantially reduces the cycle life of the battery. Numerous strategies have been employed to tackle the critical challenge of the AlPSs dissolution shuttle effect. This section highlights recent advancements aimed at mitigating the dissolution shuttle problem of AlPSs, focusing on the design of cathode design, separator modification, and innovations in electrolyte engineering.

4.1. Cathode Design

In the early stages of research, the primary strategy for capturing AlPSs focused on using porous carbon materials with high surface areas and numerous pores. This sulfur-carbon (S/C) composite utilizes porous conductive carbon as support, achieved by pouring molten sulfur (S_8) into the carbon matrix. This method is designed to confine the entire sulfur reduction reaction within the carbon pores, which helps to minimize the dissolution of AlPSs in the electrolyte. Studies have shown that porous carbon materials effectively prevent the dissolution and shuttling of AlPSs.

Hollow carbon, produced using the template method, has been utilized in Al-S batteries. These cave-like porous structures

form a cage-like cavity that accommodates sulfur and AlPSs, thereby reducing the shuttle effect problem.[98] However, relying solely on physical confinement is inadequate for preventing the dissolution and shuttling of AlPSs during prolonged cycling, as non-polar carbon materials have limited capacity to adsorb AlPSs. The weak intermolecular forces allow soluble high-order AlPSs to diffuse from the porous carbon into the electrolyte. Acknowledging the polar nature of AlPSs, researchers have utilized the strong chemical interactions between polar sulfur hosts and AlPSs to prevent their diffusion and shuttling. For example, a nitrogen-doped hierarchical porous carbon material with a surface area of up to 2513 $m^2\ g^{-1}$ has been successfully created. The graded pore structure of this material promotes efficient electrolyte transport and securely holds sulfur nanoparticles. Additionally, nitrogen doping enhances charge transfer and stabilizes aluminum sulfide, thereby improving the anode's electrochemical stability.[72] To optimize sulfur loading, Fan et al. employed zinc nitrate hexahydrate as a pore former to synthesize nitrogen-doped three-dimensional porous carbon materials (N-C/S) via high-temperature carbonization.[85] Characterization results show that the spatial confinement of these 3D porous structured materials is beneficial for sulfur loading, while nitrogen incorporation improves the chemical adsorption of sulfur. Consequently, Al-S batteries using N-C/S composite positive electrode materials demonstrate exceptional performance, achieving an excellent discharge-specific capacity of 1800 mAh g^{-1} in the first cycle.

Comparable results have been obtained with high molecular weight polymer materials containing highly electronegative elements. Sulfur and polyacrylonitrile were used as precursors, which were calcined in an inert atmosphere at 300–400 °C to produce highly reversible positive electrode materials known as SPAN. Research has demonstrated that short-chain sulfur molecules ($-S_{2/3}^{-}$) are covalently bonded to the side chains of SPAN. This unique structure enables the direct generation of the final discharge product, bypassing the formation of intermediate products during the discharge process. This structural design fundamentally prevents the dissolution and diffusion of polysulfides, maximizing the utilization of active materials in the battery system.[12,99] Additionally, the six-membered ring structure formed through thermal decomposition polymerization contains a strongly electronegative nitrogen element, which serves as an effective chemical anchoring site for polysulfides.[35] It is important to note that while research on SPAN in Li-S systems has progressed, its application in Al-S systems has received insufficient attention. To date, there has only been one study involving SPAN-positive electrode materials using IL electrolytes. Based on the available data, the electrochemical performance of SPAN in IL lacks objectivity, and the underlying reaction mechanisms require further investigation to develop highly reversible Al-S batteries.[86]

Beyond creating porous carbon materials with heteroatoms, dispersing sulfur in polar organic frameworks, such as metal–organic frameworks (MOFs) and their derivatives, is another effective approach to stabilizing AlPSs. MOFs have desirable characteristics, including tunable ligands and adjustable porosity. The use of open coordination metal sites in MOFs to adjust the chemical adsorption environment has been extensively applied in battery material research. For example, employing cobalt-based MOFs (ZIF-67-700) and their derivatives as sulfur hosts significantly reduces voltage hysteresis in Al-S batteries. Importantly, the cycling stability of both S@ZIF-67 and S@ZIF-67-700 is significantly better than that of pure sulfur used as the positive electrode. This enhancement is attributed to ZIF-67-700′s ability to serve as an anchoring site for sulfur (S_8) and polysulfides (Al_2S_3, Al_2S_6, Al_2S_{12}, and Al_2S_{18}), effectively hindering detrimental dissolution and shuttling processes.[100]

Given the limited capacity of adsorption sites to capture AlPSs, relying solely on adsorption is insufficient to prevent the dissolution and diffusion of soluble active materials. To fully address these issues, implementing suitable catalytic measures in conjunction with adsorption is necessary. Utilizing appropriate catalysts can enhance the reaction kinetics of sulfur conversion by reducing the lifespan of intermediate soluble AlPSs, thereby maximizing sulfur utilization. For instance, when using titanium nitride (TiN) as a catalyst in a cathode consisting of nitrogen-doped graphene (NG) and sulfur. The battery's initial capacity reaches ≈950 mAh g^{-1} and remains ≈500 mAh g^{-1} after 200 cycles at a current density of 100 mA g^{-1}. This remarkable capacity retention is responsible for the TiN-NG interface, which functions as a potent adsorption site for polar AlPSs, thereby inhibiting their shuttling. Furthermore, it is important to note that TiN's catalytic effect lowers the decomposition reaction barrier of polysulfides, enhancing their redox reaction kinetics (**Figure 10a**).[97] By virtue of their high conductivity and catalytic features, transitional metal nanoparticles have also been the focus of many researchers. Transition metal nanoparticles have also been extensively studied for their high conductivity and catalytic properties. By incorporating cobalt (Co) atoms into nitrogen-doped graphene (CoNG) as an electrochemical catalyst within the cathode composite materials, the voltage hysteresis of the CoNG-S composite was significantly reduced to 0.76 V, achieving a reversible specific capacity of 1631 mAh g^{-1} at a current density of 0.2 A g^{-1}, with a sulfur utilization rate exceeding 97%.[84] To address the challenges of large volume change and slow conversion of AlPSs during the cycle in Al-S batteries, a porous Co-N-doped graphene-carbon nanotube (CoN-GC) hybrid was developed. This material comprises a robust hybrid of graphene and carbon nanotubes (CNTs), resulting in a 3D conductive framework that is catalyzed by cobalt. The resultant porous CoN-GC showcases outstanding mechanical characteristics, accommodates significant sulfur loading, and mitigates the volume change of the electrode. The presence of the active site CoN_4 is crucial for facilitating rapid electron transport, adsorption, and catalysis of AlPSs. Capitalizing on these benefits, Assembled batteries employing S@CoN-GC cathode materials have demonstrated over 2000 cycles at a current density of 300 mA g^{-1}, sustaining a remarkable specific capacity of 315 mAh g^{-1}.[82] Besides cobalt nanoparticles, other transition metal nanoparticles with 3d orbitals have been used to address the shuttling problem of sulfur species. For example, copper-synergistic MoO_2-based nanohybrids (Cu/MoO_2@C) were developed as cathode materials for rechargeable Al-S batteries following the pyrolysis of polymolybdate-based MOFs (POMOFs). This material's advantage is its uniform dispersion of copper within the carbon matrix, creating a conductive network that enhances rapid charge transfer throughout the electrode and improves the conversion of polysulfides. Additionally, MoO_2 effectively adsorbs the small

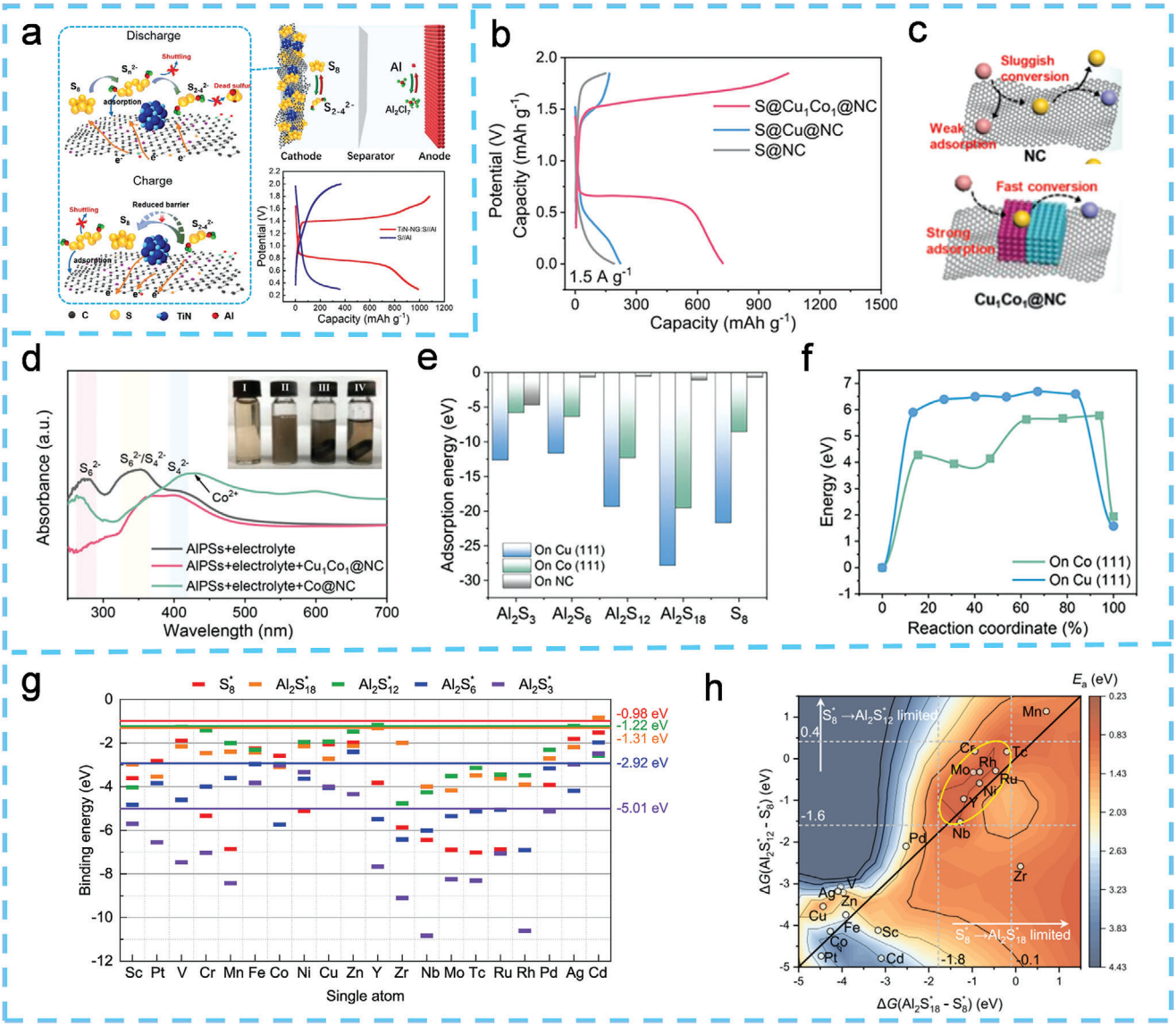

Figure 10. a) Working principle and charge–discharge curve of TiN-NG: S//Al battery. Reproduced with permission.[97] Copyright 2022, Elsevier. b) Charge–discharge curves of S@Cu_1Co_1@NC, S@Cu@NC, S@NC cathode. c) Mechanism of action of NC, Cu_1Co_1@NC on sulfur species. d) UV–vis spectra of AlPSs solutions before and after the addition of Cu_1Co_1@NC and Co@NC powders. e) Adsorption energies of S_8, Al_2S_{18}, Al_2S_{12}, Al_2S_6 and Al_2S_3 on Cu, Co and NC substrates. f) Energy profiles of Al_2S_3 decomposition on Cu and Co substrates. Reproduced with permission.[67] Copyright 2024, Wiley-VCH GmbH. g) Binding energy values of S_8 and Al_2S_n species on SA@$Ti_3C_2O_2$ nanosheets. h) Active volcano diagram determined by calculating ΔG (Al_2S_{18}* – S_8*) and ΔG (Al_2S_{12}* – S_8*). Reproduced with permission.[41] Copyright 2022, American Chemical Society.

quantities of generated polysulfides, facilitating bidirectional conversion reactions of AlPSs during both charging and discharging. The synergistic catalysis from copper clusters and MoO_2 enables the composite cathode material to achieve high sulfur utilization and conductivity.[101] Recently, Yu et al. demonstrated a bimetallic modified nitrogen-doped carbon (Cu_1Co_1@NC) as a positive electrode material for Al-S batteries, combining the benefits of adsorbed copper, catalytic cobalt, and a conductive nitrogen-doped carbon matrix.[67] As shown in Figure 10b, Cu_1Co_1@NC exhibits significantly higher specific capacity and lower overpotential compared to conventional nitrogen-doped carbon. Results from UV–vis light analysis and visual adsorption experiments indicate that the AlPSs solution with added Cu_1Co_1@NC becomes clearer, demonstrating the material's significant adsorption effect on AlPSs (Figure 10c,d). The DFT calculations of the optimized adsorption configurations for S_8, Al_2S_{18}, Al_2S_{12}, Al_2S_6, and Al_2S_3 on Cu@NC, Co@NC, and NC revealed that Cu@NC matrix displayed more negative adsorption energies for sulfur-related species, indicating that the copper component in the synthesized positive electrode material has a strong potential for AlPSs adsorption (Figure 10e). Furthermore, the energy required for the decomposition of Al_2S_3 is clearly illustrated in Figure 10f. The dissociation barriers for Al_2S_3 on Co (111) and Cu (111) are measured at 5.8 and 6.7 eV,

respectively. This suggests that the cobalt unit in Cu_1Co_1@NC plays a key role in catalyzing the sulfur species conversion, which prevents the loss of active materials during the formation of Al_2S_3. Consequently, S@Cu_1Co_1@NC maintains an impressive capacity of 317.5 mAh g^{-1} even after 320 cycles at a current density of 1.5 A g^{-1}.

To better understand the interaction characteristics between sulfur hosts with catalytic anchoring effects and AlPSs at a microscopic level, theoretical simulations were conducted to identify suitable catalytic sites. Twenty single transition metal (TM) atoms were embedded in MXene ($Ti_3C_2O_2$) nanosheets, and the role of single-atom-supported $Ti_3C_2O_2$ in generating AlPSs was examined from multiple perspectives. The theoretical analysis results indicate that Y, Nb, Mo, and Tc@$Ti_3C_2O_2$ present lower energy barriers for sulfur conversion in Al-S batteries, thereby facilitating a rapid sulfur reduction reaction process (Figure 10g). Additionally, by using the difference in free energy between S_8 and Al_2S_{18}/Al_2S_{12} as a descriptor, kinetic activity volcano plots were constructed with centers at 1.19 eV and 0.96 eV, respectively. These plots illustrate the interaction mechanism between Al_2S_n and the single-atom anchor material (Figure 10h).[41] This theoretical investigation provides new insights into the behavior of sulfur-loaded MXene materials integrated with single-atom catalysts and their role in suppressing AlPSs.

4.2. Separator Modification

The separator is an important part of the battery, serving not only to allow the passage of electrolyte ions but also to isolate the cathode and anode to avoid short-circuit problems caused by direct contact. Furthermore, in metal-sulfur batteries, the separator functions as a barrier that hinders or slows the shuttling of AlPSs.[103,104] Modifying the separator, as opposed to constructing a complex sulfur-positive electrode structure, is generally more scalable and applicable. In the Li-S battery system, various separator modification methods have been utilized effectively to reduce the shuttling of high-order lithium polysulfides.[65,105] However, this approach has been infrequently investigated in Al-S battery systems. To date, only a limited number of studies have explored separator modification strategies to mitigate the detrimental shuttling of AlPSs. Research has shown that incorporating suitable chemical additives or physical barriers on the separator surface can effectively reduce the shuttling of AlPSs, thereby enhancing sulfur retention over thousands of cycles, which is crucial for developing Al-S battery materials with high active material utilization.

It has been demonstrated that modifying the separator can alter its original physical and chemical properties, thereby impacting the performance of the battery. A thin layer of single-walled carbon nanotube (SWCNT) coating, known as SWCNT-GF, was applied to a glass fiber separator as a secondary barrier, and its effectiveness in inhibiting AlPSs shuttling was evaluated (**Figure 11a**). For comparison, an uncoated glass fiber separator (GF) was also prepared for the Al-S battery (Figure 11b). Electrochemical test results indicate that both batteries equipped with SWCNT-GF and GF separators exhibited similar discharge-specific capacities at a rate of C/20. However, the discharge capacity of the battery using a GF separator declined rapidly to below 300 mAh g^{-1} after only two cycles. Conversely, although the discharge capacity of the battery with SWCNT-GF also decreased gradually over cycles, a comparison during the first 10 cycles clearly demonstrated that the SWCNT-GF battery exhibited superior cycle stability. This difference can be attributed to the large spatial fiber structure of SWCNTs in the separator layer, whose strong conductive matrix provides a buffering space for elemental S and its redox products. This structural design effectively reduces the solubility of electrode materials in the electrolyte, resulting in improved sulfur utilization.[55]

To improve the conversion efficiency of polysulfides and prevent AlPSs from shuttling, many studies have concentrated on creating catalytic active sites within the separator modification layer. For example, a cobalt-anchored 3D nitrogen-doped carbonaceous network (Co@CMel-ZIF) was developed as a separator modification layer (Co@CMel-ZIF@GF/D) by carbonizing a mixture of ZIF-7, melamine, and $CoCl_2$ to tackle the shuttling issue of AlPSs in Al-S batteries. Co@CMel-ZIF provides abundant nitrogen-related catalytic sites that greatly promote the absorption of AlPSs, consistent with results from UV–vis spectra of the solution with AlPSs added (Figure 11d). Consequently, the Al-S battery constructed with the modified separator exhibited a discharge capacity of 503 mAh g^{-1} after 150 cycles at 20 °C (Figure 11e).[56] Additionally, Sun et al. incorporated an interconnected self-supporting iron single-atom interlayer on a porous nitrogen-doped carbon nanofiber (FeSAs-NCF) within the separator. This layer acts as both a catalyst and a chemical barrier in the battery system (Figure 11g).[102] The presence of iron in the structure, as atomically dispersed Fe-N_4, was confirmed through aberration-corrected high-angle annular dark field scanning transmission electron microscopy and X-ray absorption near-edge structure analysis. The iron active centers, atomically dispersed on the separator, can adsorb AlPSs, speed up reaction kinetics, prevent the shuttle effect, and support the reversible conversion of AlPSs. This overall enhancement improves the electrochemical performance of Al-S batteries (Figure 11f). The Al-S battery utilizing FeSAs-NCF demonstrated a low overpotential and an improved specific capacity of 780 mAh g^{-1} (Figure 11c). Some researchers have proposed covalently grafting the metallocene prototype, ferrocene (FeCp2), onto the glass fiber (GF) separator.[106] Besides providing excellent electrolyte affinity and ion permeation selectivity, the carefully modified separator layer features a negatively charged cyclopentadienyl group in FeCp2 that effectively binds to Al^{3+} in polysulfides through cation-π interactions, reducing the shuttling effect. Furthermore, the FeCp2@GF separator regulates both the deposition and stripping of aluminum while managing interfacial soluble polysulfides. Consequently, the FeCp2@GF separator facilitates a long-lasting Al-S battery with a lifespan of up to 500 cycles.

4.3. Electrolyte Engineering

Although significant advancements have been made in cathode materials and separators to address the shuttling effect of polysulfides, it is important to recognize that solid electrolytes can effectively eliminate the formation and diffusion of polysulfides, thereby minimizing sulfur material loss and enhancing the cycle stability of soluble sulfur-based batteries.[108,109] To date, only

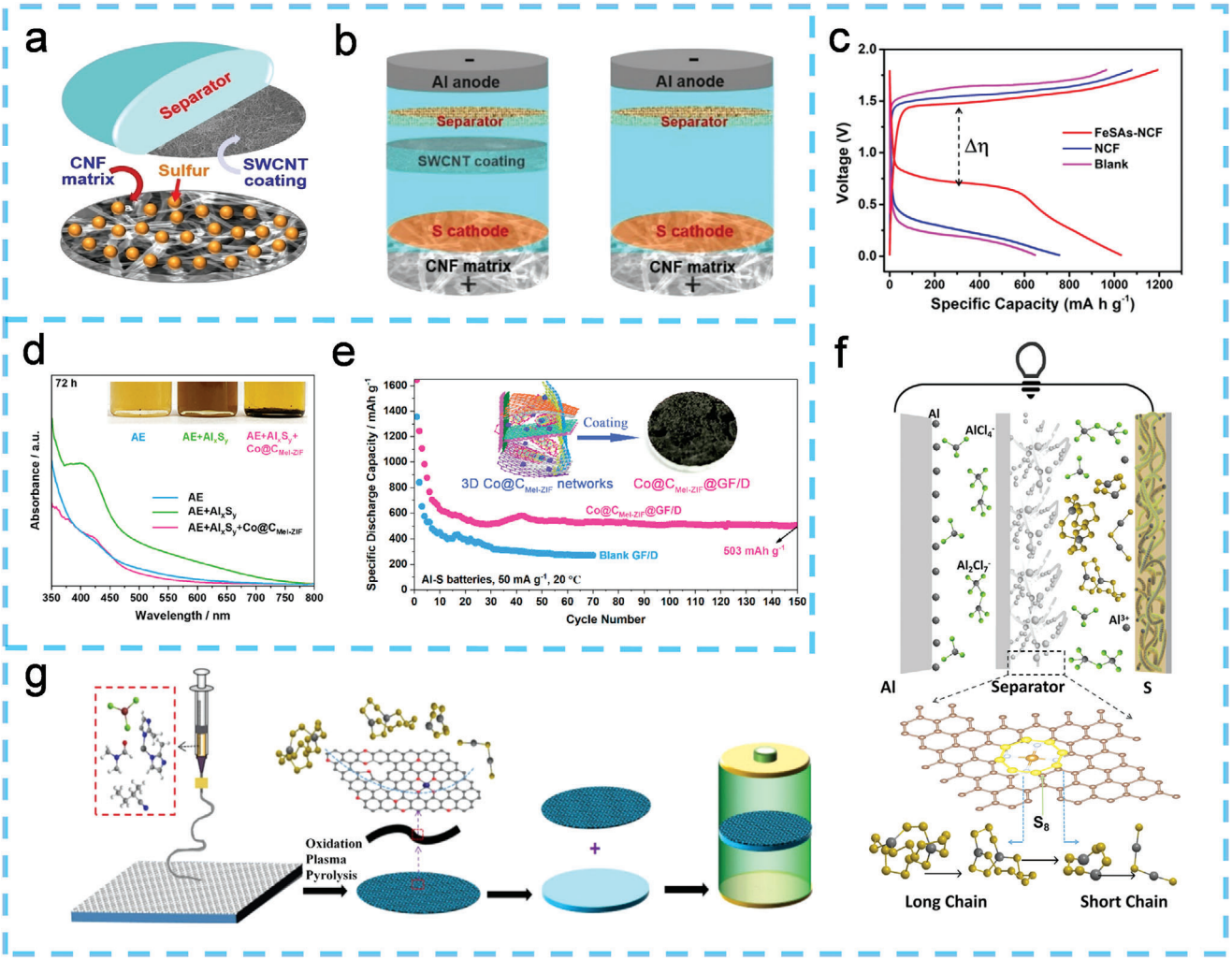

Figure 11. a) Schematic diagram of the cathode-diaphragm assembly of a room temperature Al-S battery. b) Schematic diagram of a battery with and without SWCNT coating on the separator. Reproduced with permission.[55] Copyright 2017, WILEY-VCH Verlag GmbH & Co. KGaA, Weinheim. c) Charge and discharge curves of blank, NCF, and FeSAs-NCF materials. Reproduced with permission.[102] Copyright 2022, The Authors, published by Springer. d) UV–vis spectra of blank electrolyte, electrolyte dissolved with polysulfide, and after adsorption with Co@CMel-ZIF powders for 72 h. The inset shows the picture of the solutions. e) Electrochemical performance of blank and Co@CMel-ZIF modified separator Al-S batteries at 20 °C. Reproduced with permission.[56] Copyright 2023, American Chemical Society. f) Schematic diagram of shuttle effect suppression in a battery with FeSAs-NCF as a cathode. g) Synthesis diagram of FeSAs-NCF. Reproduced with permission.[102] Copyright 2022, The Authors, published by Springer.

three research papers have addressed solid electrolytes in Al-S batteries, indicating a need for further investigation in this area. In other sulfur-based battery systems, the use of (quasi) solid electrolytes has proven effective in alleviating the shuttling effect of polysulfides, resulting in stable cycling performance. However, solid electrolytes exhibit greater kinetic sluggishness compared to liquid electrolytes, which poses challenges for the practical implementation of (quasi) solid-state Al-S batteries. To address this challenge, Jiao et al. combined cobalt-nitrogen co-doped graphene (CoNG) with electrocatalysts and IL encapsulated in a MOF to develop a quasi-solid electrolyte (IL@MOF).[90] This combination resulted in a small voltage gap of 0.43 V and a high discharge plateau of 0.9 V (**Figure** 12a,b). Moreover, the quasi-solid-state Al-S battery, utilizing a S@CoNG cathode and IL@MOF electrolyte, achieved a specific capacity of 820 mAh g^{-1} in the first cycle, with a capacity retention rate of 78% after 300 cycles. This performance was ascribed to the cooperation effects of the sulfur host material and the solid electrolyte. Specifically, the synthesized S@CoNG structure contains uniformly distributed Co-N_4 active sites, which facilitates the dissociation of active ions in $Al_xCl_y^-$ and the cleavage of S—S bonds, thereby significantly accelerating the sulfur reaction kinetics (Figure 12d,e). Additionally, the narrow and abundant channels in the MOF within IL@MOF, filled with IL ions, enable rapid transport of active ions and effectively suppress the shuttling effect of polysulfides, thereby stabilizing reversible sulfur conversion (Figure 12c).

Subsequently, the researchers explored the incorporation of platinum nanoparticles to modify the sulfur host material, successfully developing an electrocatalytically assisted gel polymer electrolyte (GPE) Al-S battery with platinum/nitrogen co-doped graphene (PtNG) as the cathode, paired with a MOF-filled gel polymer electrolyte as the solid electrolyte (Figure 12f).

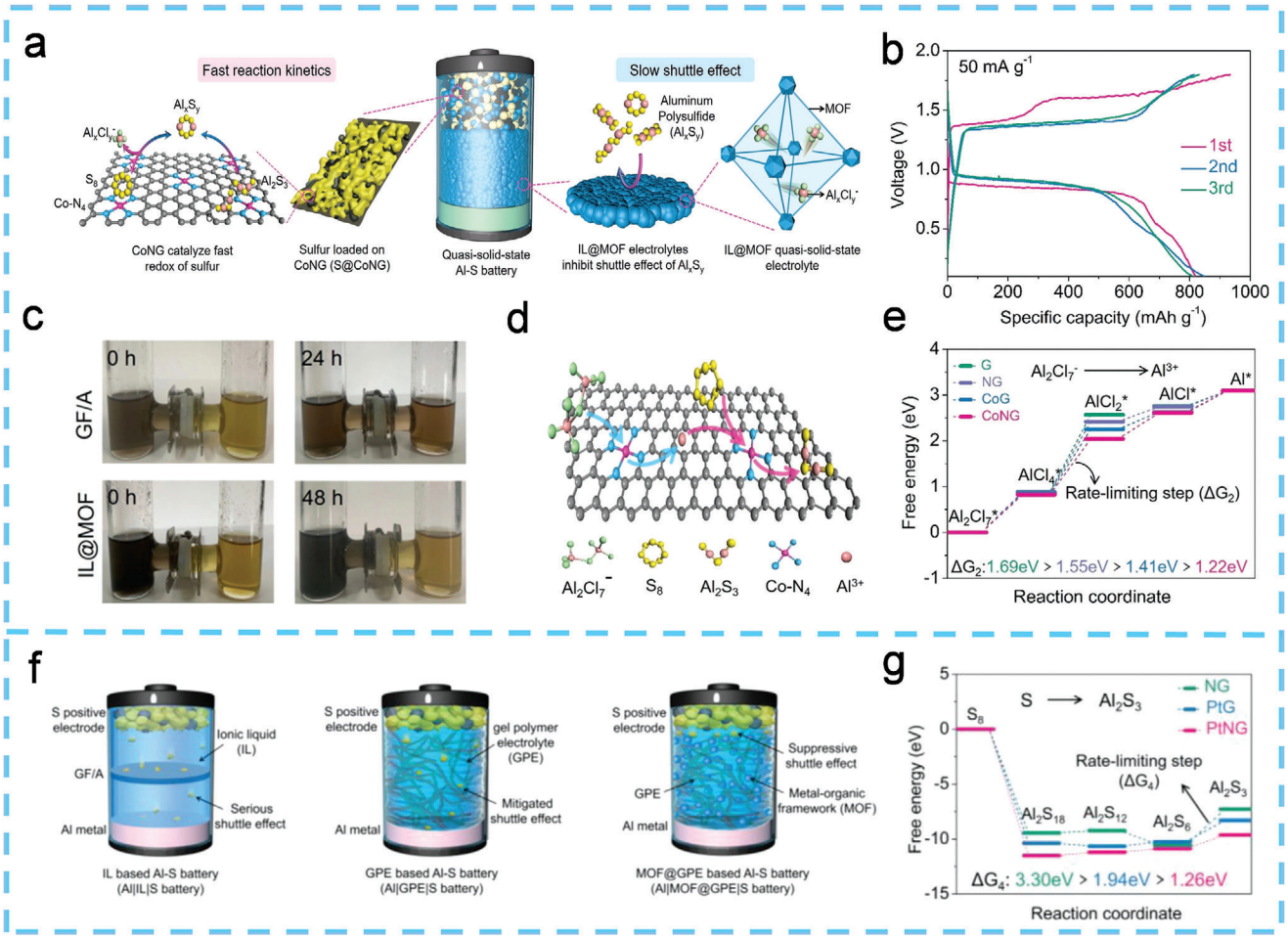

Figure 12. a) Schematic diagram of a quasi-solid-state Al-S battery and the working mechanism. b) Charge–discharge curves of AlIIL@MOFIS@CoNG batteries. c) Permeability testing of GF/A diaphragms and IL@MOF. d) Schematic diagram of sulfur reduction on CoNG substrates. e) Dissociation energy barriers of chloroaluminate clusters on G, NG, CoG, and CoNG substrates. Reproduced with permission.[90] Copyright 2022, Wiley-VCH GmbH. f) Schematic diagrams of Al|IL|S, Al|GPE|S and Al|MOF@GPE|S batteries and their operation mechanisms. g) Energy profiles for the reduction of sulfur on NG, PtG, and PtNG substrates. Reproduced with permission.[107] Copyright 2023, Elsevier Ltd.

The assembled MOF@GPE-based Al-S battery demonstrated excellent cycling performance, achieving a small voltage gap of 0.38 V and a high discharge voltage plateau of 0.95 V. This improvement is attributed to the introduction of Pt and N active catalytic sites, which reduce the energy barrier for the conversion of sulfur species (Figure 12g).[107] This finding validates the feasibility of integrating electrocatalysts with MOF-based gel electrolytes, offering new insights into enhancing the rechargeability of Al-S batteries. To address the challenge of large-scale production of Al-S batteries, which is hindered by the absence of suitable cathode current collectors, Jiao et al. combined IL-impregnated metal–organic framework solid electrolytes (MSE) with polyacrylamide gel electrolytes to create large-scale solid electrolytes (MSE@GPE).[110] The assembled Al-S soft-pack battery demonstrated a reversible capacity of 288 mAh and a battery-level energy density exceeding 90 Wh kg^{-1}. Furthermore, the MSE@GPE electrolyte effectively suppressed the shuttling effect of polysulfides, enabling the Al-S soft-pack battery to achieve a cycle life exceeding 400 cycles, with a capacity retention rate of 80%. Notably, the battery pack, which consisted of eight solid-state Al-S batteries, was able to reliably charge smartphones and power electric fans, demonstrating practical applicability. This study presents a feasible pathway toward realizing truly practical Al-S batteries.

5. Anode Protection Strategies

Although extensive research on cathode materials and electrolytes for Al-S batteries has led to improved electrochemical performance, the battery's poor cycle life remains inadequate for the long-term requirements of large-scale energy storage applications. The primary cause of this issue is battery failure due to aluminum dendrite growth and the bulk pulverization of the anode. The electrochemical redox reaction occurring at the surface of the aluminum anode during cycling can be represented as: $Al+7AlCl_4^- \rightarrow 4Al_2Cl_7^- + 3e^-$. Overall, the long-term cycle stability of Al-S batteries relies on the stable plating and stripping behavior of the aluminum anode. Ideally, the processes of solvation of aluminum from the metal surface to the electrolyte and desolvation of its ionic state should occur seamlessly

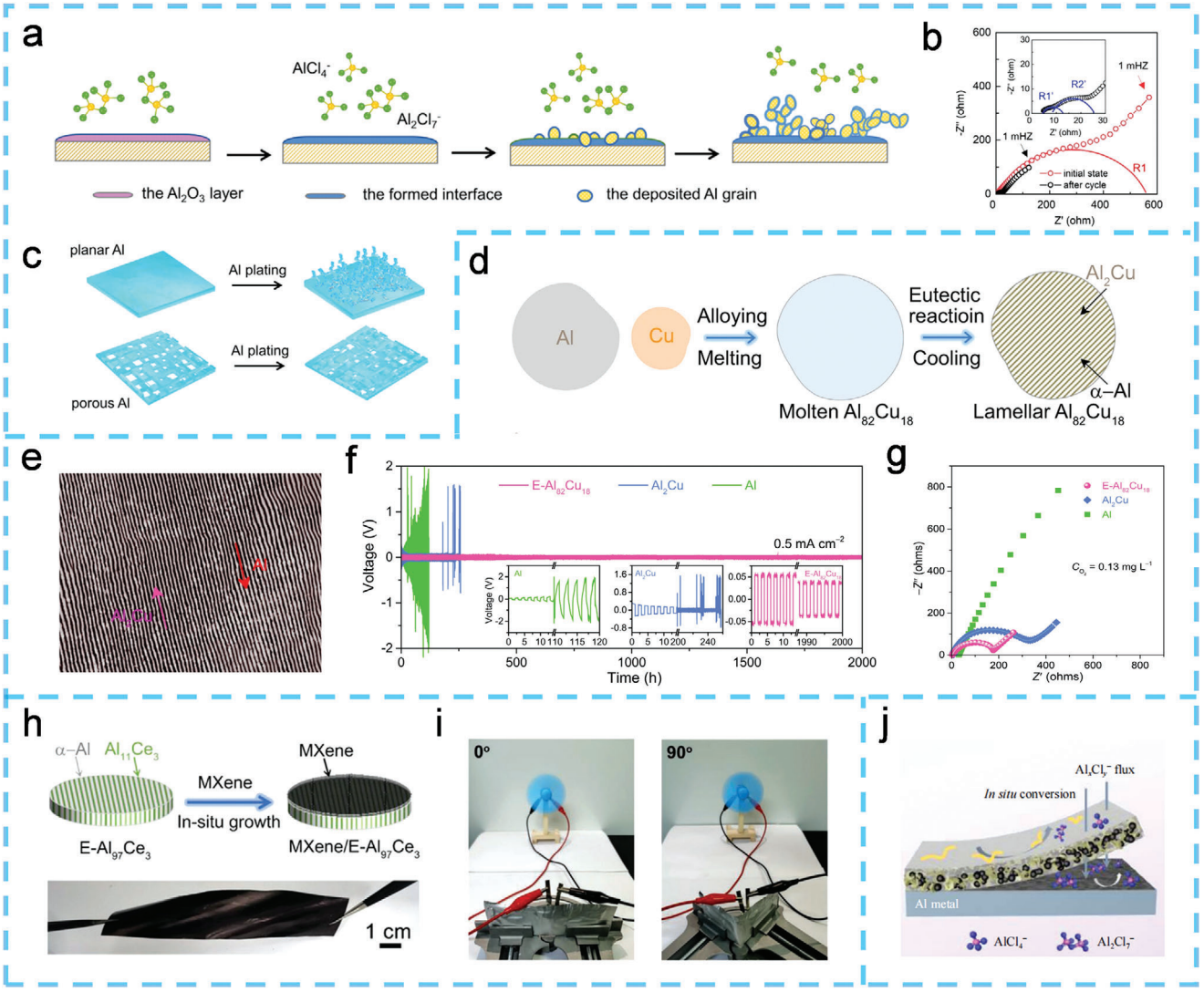

Figure 13. a) The scheme for the dissolution of the Al_2O_3 layer, the evolution of SEI, and the dendrite growth. b) The EIS curve of planar Al anode at the first cycle and the 10th cycle. c) Scheme of the Al plating processes on planar Al and porous Al. Reproduced with permission.[111] Copyright 2020, Elsevier B.V. d) Preparation process of E-$Al_{82}Cu_{18}$ alloy. e) Optical micrograph of E-$Al_{82}Cu_{18}$ alloy plate. f) Long-term cycling stability of Al stripping/plating for symmetric battery based on E-$Al_{82}Cu_{18}$, Al_2Cu, and Al electrodes at 0.5 mA cm^{-2}. g) EIS spectra of asassembled E-$Al_{82}Cu_{18}$, Al_2Cu, and pure Al symmetric battery in 2 M $Al(OTF)_3$ aqueous electrolyte with CO_2 = 0.13 mg L^{-1}.Reproduced with permission.[112] Copyright 2022, The Authors, published by Springer Nature. h) Synthesis of MXene/E-$Al_{97}Ce_3$ materials. i) Optical photographs of soft-package MXene/E-$Al_{97}Ce_3$||AlxMnO_2/C battery at bending angles of 0° and 90° when powering an electric mini-fan. Reproduced with permission.[113] Copyright 2022, Wiley-VCH GmbH. j) Mechanism of action of Al/TB modified electrode. Reproduced with permission.[114] Copyright 2022, Springer Nature.

throughout the battery's charging and discharging cycles. However, the non-directional deposition of Al^{3+} on the Al metal surface after desolvation leads to dendrite formation, which can cause internal short circuits and ultimately battery failure. In addition, the corrosive nature of the acidic electrolyte, combined with uneven stripping of the aluminum, inevitably results in pitting. Over repeated charging and discharging processes, the aluminum anode can degrade into aluminum powder. These corrosion and degradation issues gradually compromise the integrity of the aluminum anode, ultimately resulting in capacity loss and reduced cycle life of the Al-S batteries. Consequently, protecting and optimizing the aluminum anode is crucial for achieving long-lasting Al-S batteries. Current research on strategies for protecting the aluminum anode in the Al-S system primarily focuses on the application of aluminum oxide films and promoting uniform deposition of Al^{3+}. Researchers have differing views on whether an aluminum oxide (Al_2O_3) film on the surface of the aluminum anode is beneficial for the electrochemical performance of the batteries. Yang et al. directly observed significant aluminum dendrite growth on planar aluminum metal anodes using in situ optical microscopy, indicating that the oxide layer hinders the transfer of Al^{3+} and the redox reaction. [111] As illustrated in **Figure 13a**, before dendrite formation, the Al_2O_3 layer on the aluminum surface dissolves in the IL electrolyte, resulting in the formation of a solid electrolyte interphase with Al-Cl and Al-O species on the anode surface (Figure 13b).

With increasing aluminum plating time, dendrites grow progressively, creating an unstable aluminum/electrolyte interface during the plating and stripping cycles. To address this issue, researchers designed a porous aluminum anode to suppress dendrite growth. This interconnected pore structure reduces local current density and disperses ion flux, promoting uniform aluminum deposition (Figure 13c).

Similar studies have indicated that appropriate concentrations of $Al_2Cl_7^-$ can induce electrochemical microcorrosion of aluminum metal anodes, which helps remove the inert oxide film from the aluminum surface and enhances charge/discharge performance.[115] In contrast to previous reports, Gao et al. found that the Al_2O_3 film can effectively limit the growth of aluminum dendrites, thereby improving the cycle stability of the aluminum anode.[116] By comparison, the surface Al_2O_3 film is critical for protecting the aluminum anode by reducing nucleation sites, controlling dendrite growth, and preventing electrode disintegration. With the aid of this protective aluminum oxide film, the aluminum-graphite full battery achieved stability for up to 45 000 cycles.

Another strategy to inhibit aluminum dendrite growth is to promote uniform deposition of Al^{3+}. Alloys have shown effectiveness in reducing dendrite growth and extending the lifespan of aluminum batteries by ensuring uniform ion flux and facilitating ion transport. Jiang et al. synthesized a eutectic $Al_{82}Cu_{18}$ (at%) alloy (E-$Al_{82}Cu_{18}$) through a eutectic reaction, achieving dendrite-free aluminum deposition during stripping and plating cycles in aqueous electrolytes (Figure 13d).[112] Optical micrographs of the E-$Al_{82}Cu_{18}$ alloy plate reveal the formation of an ordered layered nanostructure after an in situ eutectic solidification reaction, consisting of alternating monometallic α-Al and intermetallic Al_2Cu layers, which create periodic local Al/Al_2Cu galvanic couples (Figure 13e). The less precious α-Al flakes serve as electroactive materials in the anode electrode, providing Al^{3+} charge carriers, while the more precious Al_2Cu flakes act as 2D nanopatterns to guide aluminum, facilitating highly reversible stripping and plating. Consequently, the E-$Al_{82}Cu_{18}$ electrode exhibits excellent aluminum stripping/plating stability for over 2000 h and a low overpotential (Figure 13f,g). Following this, a uniform MXene-grafted E-$Al_{97}Ce_3$ alloy was developed to suppress side reactions at the aluminum anode and facilitate Al^{3+} transport by mitigating the passivating oxide layer (Figure 13h). MXene serves as a stable solid electrolyte interphase to suppress side reactions, while the layered nanostructured E-$Al_{97}Ce_3$ utilizes the coexisting α-Al metal and intermetallic $Al_{11}Ce_3$ sheets to achieve directional aluminum stripping and deposition. The MXene/E-$Al_{97}Ce_3$ hybrid electrode realizes a highly flexible and dendrite-free aluminum-based anode in a low-oxygen-concentration aqueous aluminum trifluoromethanesulfonate ($Al(OTF)_3$) electrolyte. Notably, the excellent flexibility of the electrode material allows the assembled soft-pack battery to maintain outstanding airtightness when bent at various angles, effectively powering a micro fan (Figure 13i).[113]

In addition to alloying the aluminum anode, applying a protective coating to the anode surface is also considered an effective means of anode protection. Coating the aluminum anode with graphite to regulate the plating and stripping behavior results in improved cycling stability and lower overpotential compared to a bare aluminum anode. The aluminum ions preferentially plate on the graphite layer rather than the aluminum substrate. Furthermore, the rough texture of the graphite coating, with its numerous voids, enhances current uniformity and accommodates volume changes in aluminum, significantly inhibiting dendrite growth.[117] Fang et al. proposed a self-supporting nitrogen-doped carbon rod array (NCRA) as a framework for reversible aluminum plating and stripping.[118] The nitrogen-containing functional groups and matrix structure effectively regulate aluminum nucleation and inhibit dendrite formation. During plating, aluminum metal evenly covers the surface of the NCRA matrix, which is fully restored after stripping. This stable matrix structure results in a corrosion-resistant and non-powdering aluminum metal anode. In the Al-S system, optimizing anode protection also entails inhibiting parasitic reactions of active materials at the aluminum anode. This approach aims to improve the utilization of active materials in the battery system while preventing contamination of the aluminum anode that could affect the battery's service life. To address severe corrosion of the aluminum anode, Jiao et al. proposed a modified layer that combines electrochemically inert TiB_2 with carbon black nanoparticles to protect the exposed aluminum electrode.[114] This innovative electrode design promotes uniform nucleation and growth of Al^{3+} and leverages the oxygen-containing components in TiB_2 crystals to facilitate the in situ conversion of soluble tellurium species through Te—O bonds, thereby preventing the loss of tellurium at the aluminum anode (Figure 13j). Furthermore, the design of electrolytes has been explored as a method to protect aluminum anodes. By incorporating alkaline chlorides (LiCl, NaCl, and KCl) into the electrolyte, a thicker, electronically insulating solid electrolyte interface (SEI) containing $Na_xAl_yO_2$ forms on the aluminum anode. This SEI can inhibit the deposition of low-solubility Al_2S_3 and/or short-chain polysulfides, thereby avoiding surface contamination of the aluminum anode and further improving battery cycle performance. This approach is significant for the development of long-life Al-S batteries.[93]

6. Conclusions and Prospects for Practical Application

Given that sulfur and aluminum offer high energy density and low cost, there is renewed interest in developing safe, reliable, and affordable energy storage systems. Over the past decade, research on Al-S batteries has significantly narrowed the performance gap between this new energy storage system and other metal-sulfur batteries, such as Li-S and Na-S batteries. The specific electrochemical performance of the Al-S batteries is shown in **Table 1**. However, similar to other metal-sulfur batteries, the Al-S battery system faces several common challenges. These challenges include slow reaction kinetics, pronounced polysulfide shuttle effects, and uncontrolled dendrite growth on the anode electrode. To better understand potential design solutions for these issues, we examine the various components of the battery—namely, the cathode, electrolyte, separator, and anode, and specifically discuss how optimizing and modifying each component can address these persistent challenges. While addressing these fundamental electrochemical issues in Al-S batteries, it is also essential to consider efforts aimed at advancing the commercialization of these batteries. The challenges and directions for commercialization can be categorized into four key areas:

Table 1. Electrochemical performance, manufacturing parameters, and battery testing conditions for Al-S battery research from 2015 to 2024.

Cathode materials	Electrolyte	Operation temperature [°C]	Voltage window [V]	Current density	Initial specific capacity [mAh g^{-1}]	Cycle number	Residual capacity [mAh g^{-1}]	Typical energy efficiency [%]	Average discharge voltage [V]	Coulombic efficiencies [%]	Refs.
HC/S	$[AlCl_3]_{1.3}[EMICl]_1$	RT	0.01–1.7	100 mA g^{-1}	1027	28	378	17.7%	0.4	≈60	[98]
AC cloth/S	$[AlCl_3]_{1.3}[EMICl]_1$	25	0.2–1.6	50 mA g^{-1}	1320	20	1000	40.4%	0.6	–	[38]
KB/S	$[AlCl_3]_{1.3}[EMICl]_1$	RT	<1.2	50 mA g^{-1}	1400	–	–	–	≈1.1–1.2	–	[54]
TiN-NG/S	$[AlCl_3]_{1.3}[EMICl]_1$	RT	0.3–1.8	100 mA g^{-1}	993	200	500	48.6%	0.8	92	[97]
Ti_3C_2Tx/S	$[AlCl_3]_{1.3}[EMICl]_1$	RT	0.01–1.8	300 mA g^{-1}	489	280	415	31.7%	0.5	≈95	[77]
SWCNT/S	$[AlCl_3]_{1.3}[EMICl]_1$	RT	0.2–1.8	100 mA g^{-1}	1024	15	400	–	0.5	–	[119]
HPCK/S	$AlCl_3$-AcA	25	0.1–1.75	1 A g^{-1}	1583	700	405	36.5%	0.6	96.2	[72]
MWCNT/S	$AlCl_3$-AcA	RT	1.0–2.5	560 mA g^{-1}	880	400	320	–	1.65–1.85	–	[95]
MWCNT/S	$[AlCl_3]_{1.3}[EMICl]_1$-2NaCl	RT	0.01–1.5	100 mA g^{-1}	>1200	50	473	45.3%	0.6	–	[93]
CNF paper/S	$[AlCl_3]_{1.3}[EMICl]_1$	RT	0.3–1.8	C/20	1250	10	≈600	–	0.95	–	[55]
Graphene/CoS_2/S	$[AlCl_3]_{1.3}[EMICl]_1$	RT	0.01–1.8	50 mA g^{-1}	1145	38	676	–	0.3	–	[105]
S@Co/C	$[AlCl_3]_{1.3}[EMICl]_1$	RT	0.1–1.8	1 A g^{-1}	1650	200	500	38.2%	0.6	≈90	[66]
CNF/S	$AlCl_3$-Urea				2359	–	–	–	0.41	–	[120]
HKUST-1-C/S	$[AlCl_3]_{1.3}[EMICl]_1$	RT	0.1–1.8	1 A g^{-1}	1200	500	460	23.9%	0.4	95	[73]
N-C/S	$AlCl_3$-AcA	RT	0.1–2.2	–	1800	20	700	37.7%	0.6	83	[85]
CNF/S	$AlCl_3$-Urea	RT	1.0–2.4	200 mA g^{-1}	225	100	≈100	75.0%	1.8	94	[39]
C/S	$Al(OTF)_3$/LiTFSI/HCl	RT	0.3–1.7	200 mA g^{-1}	1410	30	420	35.7%	0.55	96	[63]
CoNG/S	$[AlCl_3]_{1.3}[EMICl]_1$	RT	0.1—1.8	200 mA g^{-1}	1631	10	500	–	0.75	115	[84]
SWCNT/S	$[AlCl_3]_{1.4}[Urea]_1$	RT	1.0–2.4	1A g^{-1}	≈740	100	520	–	1.6-2.0	92	[61]
Graphene/S	$[AlCl_3]_{1.3}[EMICl]_1$- 0.8dFBn	20	0.05–1.5	100 mA g^{-1}	1563	300	507	30.8%	0.5	≈83	[60]
CoNG/S	$[AlCl_3]_{1.3}[EMICl]_1$-MOF	RT	0.1–1.8	50 mA g^{-1}	820	300	640	61.7%	0.9	93	[90]
CoNG/S	$[AlCl_3]_{1.3}[EMICl]_1$−MSE@GPE	RT	0.2–1.8	0.05C	685	400	≈550	67.6%	1	≈93	[110]
Graphene/S	NaCl-KCl-$AlCl_3$	110	0.6–1.5	5C, D/2	≈550	500	≈350	78.1%	1.05	–	[40]
CNF/S	NaCl-KCl-LiCl-$AlCl_3$	85	0.2–1.6	1C, D/2	≈635	1400	542	61.9%	0.9	–	[68]
Py-MPG/S	$AlCl_3$/AcA	RT	0.01–1.8	100 mA g^{-1}	≈1500	250	370	73.8%	0.87	–	[79]
S@CMK-3	EMIBr/$AlCl_3$	RT	≈0.25–1.8	251 mA g^{-1}	1300	20	400	41.1%	0.5	–	[57]
S@CMK-3	$AlCl_3$/AcA	RT	0.05–1.8	100 mA g^{-1}	1500	60	500	40.7%	0.6	85	[62]
CNF/S	$[AlCl_3]_{1.3}[EMICl]_1$	RT	0.01–1.8	1 A g^{-1}	≈900	500	320	34.6%	0.7	90	[102]
ZIF-67-C/Al_2S_3	$[AlCl_3]_{1.3}[EMICl]_1$	RT	0.1–1.8	160 mA g^{-1}	560	100	≈400	42.0%	0.7	>95	[87]
HPCK/S	$AlCl_3$/AcA	RT	≈0.7–2.4	1 A g^{-1}	861	490	467	81.0%	1.8	–	[65]
CNF paper/S	Li^+-$[AlCl_3]_{1.3}[EMICl]_1$	RT	≈0.4–2.0	C/20	1000	50	600	40.6%	0.72	95	[58]
BN/C/S	$[AlCl_3]_{1.3}[EMICl]_1$	RT	0.05–2.2	100 mA g^{-1}	–	300	532	56.9%	1.15	94.3	[121]
ZIF-67/S	$[AlCl_3]_{1.3}[EMICl]_1$	RT	0.1–2.0	100 mA g^{-1}	≈700	50	180	26.4%	0.5	95	[100]
PtNG/S	$[AlCl_3]_{1.3}[EMICl]_1$-MOF@GPE	RT	0.1–1.8	50 mA g^{-1}	1009	300	653	64.5%	0.95	82	[107]

1) **Developing highly compatible electrolytes**. For Al-S batteries to achieve high reaction kinetics and long cycle life, it is essential to develop a suitable electrolyte that is compatible with all components of the system. The evaluation of these electrolytes should be based on several key criteria, including high chemical and electrochemical stability, a wide voltage range, high ionic conductivity, and compatibility with electrode materials. Additionally, it is crucial to maintain high and stable Al^{3+} solvation and desolvation kinetics during long-term cycling to facilitate a rapid and efficient stripping and deposition process. Based on the current development history of Al-S battery electrolytes, while aqueous electrolytes are safe and cost-effective, they face challenges such as low reversibility in the plating and stripping processes at room temperature. Furthermore, research is constrained by significant polarization and the tendency of water to decompose at low voltages. Organic ILs, such as $AlCl_3$-EMIC and its analogs (e.g., $AlCl_3$-urea/acetamide), exhibit high viscosity and low ionic conductivity at room temperature. Although several optimization strategies have been proposed to address these issues, their effectiveness has been limited. In contrast, while inorganic molten salt electrolytes have seen improvements in viscosity and ionic conductivity, they require more demanding operating conditions, making their full application in Al-S batteries challenging. Therefore, finding a suitable electrolyte to match Al-S batteries is critical for advancing practical applications. Given the current state of Al-S battery development, creating slightly soluble electrolytes may effectively address the issue of AlPSs shuttling. This electrolyte design enables the rapid diffusion of chloroaluminate ion clusters while also achieving slightly soluble or even insoluble properties for higher-order AlPSs produced during sulfur's redox reactions. This approach not only maintains rapid "solid-liquid-solid" reaction kinetics during sulfur conversion but also significantly enhances the utilization of active materials. Additionally, solid electrolytes represent a promising avenue for exploring new electrolyte options. On one hand, solid electrolytes offer higher energy density. On the other hand, they effectively mitigate short-circuit issues caused by metal dendrites. Current efforts focus on enhancing the reaction kinetics of solid electrolytes by reducing excessive interfacial resistance with electrode materials, accelerating ion transport within the solid electrolytes, and lowering the costs of these often-expensive electrolytes. From a practical perspective, the cost of electrolytes should also be a key criterion in their evaluation. Since the electrolyte constitutes a significant portion of the battery's cost, its economic viability could be crucial in determining whether Al-S batteries are suitable for large-scale production. Consequently, it is important to thoroughly investigate new electrolyte systems with good compatibility, particularly for the Al-S electrolyte system, which has substantial development potential.
2) **Revealing reaction mechanisms based on advanced in situ characterizations**. Throughout the development of Al-S batteries, a significant challenge has been the unclear mechanism of sulfur during electrochemical reactions. To create a high energy density Al-S battery system, it is essential to thoroughly understand the charging and discharging mechanisms throughout the electrochemical reaction process. Despite numerous hypotheses being proposed, most characterization methods in Al-S batteries are non-in situ, resulting in insufficient accuracy for verifying these mechanisms. Consequently, more advanced in situ or innovative characterization approaches are required to complement experiments, allowing for verification of existing hypotheses or exploration of previously unexamined mechanisms. Employing techniques such as in situ XRD, in situ Raman, in situ TEM, and extended X-ray absorption fine structure (EXAFS) allows for real-time monitoring of the electrochemical reactions of active sulfur during charging and discharging, providing valuable insights into the formation and conversion of sulfur-related species. In addition, the in situ characterization technology of single nanowires based on 1D geometry is also an effective means to explore the electrochemical energy storage mechanism. Once the electrochemical reaction mechanisms of Al-S batteries are understood, we can effectively control the reversible electrochemical redox reactions by carefully regulating the charging and discharging voltage windows. Notably, advanced characterization methods have demonstrated that sulfur can exist in a high-valent oxidation state within Al-S batteries. This indicates that a novel sulfur conversion pathway, facilitated by sulfur oxidation, may enhance the reversibility and voltage platform of batteries. Therefore, revealing the electrochemical energy storage mechanism through advanced in situ characterization methods is conducive to the development of high-energy-density Al-S batteries.
3) **Providing mechanistic insights from Theoretical simulations**. Analyzing the advantages and disadvantages of cathode materials and electrolytes for Al-S batteries is essential for advancing their future development. To address this issue, researchers typically rely on experimental methods. However, conducting numerous comparative experiments is not the most efficient approach for drawing conclusions. Such an approach is often resource-intensive, requiring significant time and labor. In fact, the number of research subjects may far exceed expectations, making it exceedingly challenging to quickly and accurately identify suitable candidates. Based on this fact, theoretical research is crucial, as it can significantly streamline experimental procedures and reduce costs. Notably, theoretical simulation methods are widely applicable across various metal-sulfur cathode systems. Utilizing DFT, numerous studies have investigated the interactions between sulfur-containing materials and sulfides at the microscopic level, demonstrating the practical value of theoretical calculations. For instance, addressing the AlPSs shuttle problem in Al-S batteries involves selecting a material that effectively adsorbs AlPSs from a wide range of sulfur host materials, which is a complex task with a substantial workload. These sulfur host materials serve as adsorption matrices for AlPSs, allowing researchers to rank them based on their adsorption energy for AlPSs. Subsequently, one or several suitable candidates can be accurately identified through experimental validation. Additionally, ab initio molecular dynamics simulation (AIMD) is an effective theoretical simulation technique. AIMD is employed to investigate the kinetic properties of electrolytes, significantly enhancing researchers' ability to understand and predict their behavior and characteristics.

4) **Constructing practical Al-S batteries**. Beyond unresolved fundamental issues, the commercialization of rechargeable Al-S batteries encounters additional challenges. Key parameters must be addressed to enhance the practical application of Al-S batteries, including increasing sulfur loading, reducing the electrolyte-to-sulfur (E/S) ratio, and enhancing current density during testing. From a practical standpoint, increasing sulfur mass loading is critical for achieving commercialization. However, this approach may lead to incomplete sulfur reactions in high-mass loading electrodes and exacerbate the AlPSs shuttle effect. Designing porous skeleton materials that incorporate adsorption or catalytic sites may offer a viable solution in the future. Besides mass loading, the electrochemical properties of the battery should also be assessed at low E/S ratios and high current densities. Currently, most studies employ very low current densities and high E/S ratios for testing, which may not address real issues. This approach could impede progress and is not conducive to advancing practical applications. Therefore, it is crucial to establish standardized testing parameters to accurately evaluate the actual electrochemical performance of the battery. Concurrently, the design configuration of the battery should be actively researched. Actual energy density can be enhanced by optimizing the binder and current collector to minimize or eliminate inactive material mass. Finally, it is important to note that most existing test data for Al-S batteries are derived from button and Swagelok battery tests. These testing setups are idealized and do not accurately represent the battery's true application potential. In contrast, soft-pack batteries are more representative of practical applications and can effectively evaluate performance degradation and safety issues associated with increased battery size. Therefore, researchers should be encouraged to conduct tests on soft-pack Al-S batteries to better simulate performance in practical application scenarios.

In summary, although the development of Al-S batteries is still in its infancy, their inherent low-cost advantage renders them highly competitive in the energy storage market. To address fundamental issues within the Al-S battery system, it is essential to employ advanced characterization methods to elucidate the electrochemical reaction mechanisms, thereby optimizing battery performance. Furthermore, to facilitate the commercialization process, testing should be conducted using parameters and devices that closely mimic actual application environments, ensuring a smooth transition from laboratory testing to potential production. Considering the current enthusiasm among researchers for Al-S battery development, there is strong reason to believe that Al-S batteries will achieve large-scale commercial deployment in the future, thanks to their significant cost advantages.

Acknowledgements

Y.W. and X.W. contributed equally to this work. The authors appreciate funding support from the National Key Research, Development Program of China (2023YFB3809304) the National Science Foundation of China (52103329), and the Key Research and Development Program of Hubei (2022BAA027).

Conflict of Interest

The authors declare no conflict of interest.

Keywords

aluminum-sulfur batteries, critical challenges, optimization strategies, practical prospects

Received: November 30, 2024
Revised: January 19, 2025
Published online: February 19, 2025

[1] S. Mallapaty, *Nature* **2020**, *586*, 482.
[2] O. J. Guerra, *Nat. Energy* **2021**, *6*, 460.
[3] N. Kittner, F. Lill, D. M. Kammen, *Nat. Energy* **2017**, *2*, 17125.
[4] S. Chu, Y. Cui, N. Liu, *Nat. Mater.* **2017**, *16*, 16.
[5] Z. Zhu, T. Jiang, M. Ali, Y. Meng, Y. Jin, Y. Cui, W. Chen, *Chem. Rev.* **2022**, *122*, 16610.
[6] T. M. Gür, *Energy Environ. Sci.* **2018**, *11*, 2696.
[7] L. Mai, X. Tian, X. Xu, L. Chang, L. Xu, *Chem. Rev.* **2014**, *114*, 11828.
[8] A. Innocenti, S. Beringer, S. Passerini, *Nat. Rev. Mater.* **2024**, *9*, 347.
[9] O. Schmidt, S. Melchior, A. Hawkes, I. Staffell, *Joule* **2019**, *3*, 81.
[10] A. B. Gallo, J. R. Simões-Moreira, H. K. M. Costa, M. M. Santos, E. Moutinho dos Santos, *Renewable Sustainable Energy Rev.* **2016**, *65*, 800.
[11] C. A. F. Nason, Y. Xu, *eScience* **2024**, *4*, 100183.
[12] J. Zhao, Y.-Y. Xiao, Q. Liu, J. Wu, Z.-C. Jiang, H. Zeng, *Adv. Funct. Mater.* **2024**, *34*, 2405358.
[13] L. Zhao, Y. Tao, Y. Zhang, Y. Lei, W.-H. Lai, S. Chou, H.-K. Liu, S.-X. Dou, Y.-X. Wang, *Adv. Mater.* **2024**, *36*, 2402337.
[14] Y. Liu, B. Qu, S. Li, X. Lian, Y. Luo, X. Shen, C. Xu, J. Wang, F. Pan, *Adv. Funct. Mater.* **2024**, *34*, 2405586.
[15] B. Long, F. Wu, Y. Li, H. Yang, W. Liu, Y. Li, Q. Li, X. Feng, Y. Bai, C. Wu, *Carbon Neutralization* **2024**, *3*, 64.
[16] M.-C. Lin, M. Gong, B. Lu, Y. Wu, D.-Y. Wang, M. Guan, M. Angell, C. Chen, J. Yang, B.-J. Hwang, H. Dai, *Nature* **2015**, *520*, 324.
[17] H. Yang, H. Li, J. Li, Z. Sun, K. He, H.-M. Cheng, F. Li, *Angew. Chem. Int. Ed.* **2019**, *58*, 11978.
[18] E. Faegh, B. Ng, D. Hayman, W. E. Mustain, *Nat. Energy* **2021**, *6*, 21.
[19] J. Meng, L. Zhu, A. B. Haruna, K. I. Ozoemena, Q. Pang, *Sci. China: Chem.* **2021**, *64*, 1888.
[20] J. Tu, W.-L. Song, H. Lei, Z. Yu, L.-L. Chen, M. Wang, S. Jiao, *Chem. Rev.* **2021**, *121*, 4903.
[21] J. Meng, H. Guo, C. Niu, Y. Zhao, L. Xu, Q. Li, L. Mai, *Joule* **2017**, *1*, 522.
[22] T. Cai, L. Zhao, H. Hu, T. Li, X. Li, S. Guo, Y. Li, Q. Xue, W. Xing, Z. Yan, L. Wang, *Energy Environ. Sci.* **2018**, *11*, 2341.
[23] H. Hong, J. Liu, H. Huang, C. Atangana Etogo, X. Yang, B. Guan, L. Zhang, *J. Am. Chem. Soc.* **2019**, *141*, 14764.
[24] W. Yao, K. Liao, T. Lai, H. Sul, A. Manthiram, *Chem. Rev.* **2024**, *124*, 4935.
[25] R. Fang, S. Zhao, Z. Sun, D.-W. Wang, H.-M. Cheng, F. Li, *Adv. Mater.* **2017**, *29*, 1606823.
[26] X. Zhang, T. Yu, S. Yang, Z. Qu, R. Xiao, G. Wang, Z. Sun, F. Li, *Adv. Funct. Mater.* **2024**, *34*, 2405122.
[27] Q. Pang, A. Shyamsunder, B. Narayanan, C. Y. Kwok, L. A. Curtiss, L. F. Nazar, *Nat. Energy* **2018**, *3*, 783.
[28] D. Meggiolaro, M. Agostini, S. Brutti, *ACS Energy Lett.* **2023**, *8*, 1300.
[29] H. Ye, Y. Li, *InfoMat* **2022**, *4*, e12291.
[30] Y. Zhang, S. Liu, Y. Ji, J. Ma, H. Yu, *Adv. Mater.* **2018**, *30*, 1706310.
[31] Y. Liang, H. Dong, D. Aurbach, Y. Yao, *Nat. Energy* **2020**, *5*, 646.

[32] S. He, D. Zhang, X. Zhang, S. Liu, W. Chu, H. Yu, *Adv. Energy Mater.* **2021**, *11*, 2100769.
[33] L. Wang, H. Shi, Y. Xie, Z.-S. Wu, *Carbon Neutralization* **2023**, *2*, 262.
[34] B. Lin, Y. Zhang, W. Li, J. Huang, Y. Yang, S. W. Or, Z. Xing, S. Guo, *eScience* **2024**, *4*, 100180.
[35] M. Klimpel, M. V. Kovalenko, K. V. Kravchyk, *Commun. Chem.* **2022**, *5*, 77.
[36] Q. Zhou, Y. Wu, J. Gautam, D. Wang, X. Jiang, Z. Ma, H. Zhang, L. Ni, G. Diao, *Coord. Chem. Rev.* **2023**, *474*, 214856.
[37] M. Faheem, A. Hussain, M. Ali, M. A. Aziz, *Chem. Rec.* **2024**, *24*, 202300268.
[38] T. Gao, X. Li, X. Wang, J. Hu, F. Han, X. Fan, L. Suo, A. J. Pearse, S. B. Lee, G. W. Rubloff, K. J. Gaskell, M. Noked, C. Wang, *Angew. Chem. Int. Ed.* **2016**, *55*, 9898.
[39] H. Li, R. Meng, Y. Guo, B. Chen, Y. Jiao, C. Ye, Y. Long, A. Tadich, Q.-H. Yang, M. Jaroniec, S.-Z. Qiao, *Nat. Commun.* **2021**, *12*, 5714.
[40] Q. Pang, J. Meng, S. Gupta, X. Hong, C. Y. Kwok, J. Zhao, Y. Jin, L. Xu, O. Karahan, Z. Wang, S. Toll, L. Mai, L. F. Nazar, M. Balasubramanian, B. Narayanan, D. R. Sadoway, *Nature* **2022**, *608*, 704.
[41] Z. Wang, X. Zheng, A. Chen, Y. Han, L. Wei, J. Li, *ACS Mater. Lett.* **2022**, *4*, 1436.
[42] N. Deka, G. K. Dutta, *Curr. Opin. Electrochem.* **2023**, *38*, 101222.
[43] L. Ma, Y. Lv, J. Wu, Y. Chen, Z. Jin, *Adv. Energy Mater.* **2021**, *11*, 2100770.
[44] X. Liu, Y. Li, X. Xu, L. Zhou, L. Mai, *J. Energy Chem.* **2021**, *61*, 104.
[45] J. Zhang, R. He, L. Jia, C. You, Y. Zhang, M. Liu, N. Tian, H. Lin, J. Wang, *Adv. Funct. Mater.* **2023**, *33*, 2305674.
[46] B. Akgenc, S. Sarikurt, M. Yagmurcukardes, F. Ersan, *J. Phys.: Condens. Matter* **2021**, *33*, 253002.
[47] L. Mai, Y. Dong, L. Xu, C. Han, *Nano Lett.* **2010**, *10*, 4273.
[48] K. Yu, X. Pan, G. Zhang, X. Liao, X. Zhou, M. Yan, L. Xu, L. Mai, *Adv. Energy Mater.* **2018**, *8*, 1802369.
[49] R. Marassi, T. M. Laher, D. S. Trimble, G. Mamantov, *J. Electrochem. Soc.* **1985**, *132*, 1639.
[50] R. Marassi, G. Mamantov, J. Q. Chambers, *J. Electrochem. Soc.* **1976**, *123*, 1128.
[51] K. A. Paulsen, R. A. Osteryoung, *J. Am. Chem. Soc.* **1976**, *98*, 6866.
[52] S. Licht, D. Peramunage, *J. Electrochem. Soc.* **1993**, *140*, L4.
[53] D. Peramunage, R. Dillon, S. Licht, *J. Power Sources* **1993**, *45*, 311.
[54] G. Cohn, L. Ma, L. A. Archer, *J. Power Sources* **2015**, *283*, 416.
[55] X. Yu, A. Manthiram, *Adv. Energy Mater.* **2017**, *7*, 1700561.
[56] C. Xu, M. Zarrabeitia, Y. Li, J. Biskupek, U. Kaiser, X. Liu, S. Passerini, *ACS Nano* **2023**, *17*, 25234.
[57] H. Yang, L. Yin, J. Liang, Z. Sun, Y. Wang, H. Li, K. He, L. Ma, Z. Peng, S. Qiu, C. Sun, H.-M. Cheng, F. Li, *Angew. Chem. Int. Ed.* **2018**, *57*, 1898.
[58] X. Yu, M. J. Boyer, G. S. Hwang, A. Manthiram, *Chem* **2018**, *4*, 586.
[59] H. Li, J. Lampkin, N. Garcia-Araez, *ChemSusChem* **2021**, *14*, 3139.
[60] C. Xu, T. Diemant, A. Mariani, M. E. Di Pietro, A. Mele, X. Liu, S. Passerini, *Angew. Chem. Int. Ed.* **2024**, *63*, 202318204.
[61] Y. Bian, Y. Li, Z. Yu, H. Chen, K. Du, C. Qiu, G. Zhang, Z. Lv, M.-C. Lin, *ChemElectroChem* **2018**, *5*, 3607.
[62] W. Chu, X. Zhang, J. Wang, S. Zhao, S. Liu, H. Yu, *Energy Storage Mater.* **2019**, *22*, 418.
[63] Z. Hu, Y. Guo, H. Jin, H. Ji, L.-J. Wan, *Chem. Commun.* **2020**, *56*, 2023.
[64] Z. Huang, W. Wang, W. L. Song, M. Wang, H. Chen, S. Jiao, D. Fang, *Angew. Chem. Int. Ed.* **2022**, *61*, 202202696.
[65] D. Zhang, W. Chu, D.-Y. Wang, S. Li, S. Zhao, X. Zhang, Y. Fu, H. Yu, *Adv. Funct. Mater.* **2022**, *32*, 2205562.
[66] Y. Guo, Z. Hu, J. Wang, Z. Peng, J. Zhu, H. Ji, L.-J. Wan, *Angew. Chem. Int. Ed.* **2020**, *59*, 22963.
[67] J. Zheng, H. Zhang, T. Xu, S. Ju, G. Xia, X. Yu, *Adv. Funct. Mater.* **2024**, *34*, 2307486.
[68] J. Meng, X. Hong, Z. Xiao, L. Xu, L. Zhu, Y. Jia, F. Liu, L. Mai, Q. Pang, *Nat. Commun.* **2024**, *15*, 596.
[69] P. Bhauriyal, S. Das, B. Pathak, *J. Phys. Chem. C* **2020**, *124*, 11317.
[70] W. A. Appiah, H. Li, J. Lampkin, J. M. García-Lastra, *J. Power Sources* **2022**, *529*, 231254.
[71] A. Bhowmik, D. Carrasco-Busturia, P. Jankowski, R. Raccichini, N. Garcia-Araez, J. M. García-Lastra, *J. Phys. Chem. C* **2022**, *126*, 40.
[72] D. Zhang, X. Zhang, B. Wang, S. He, S. Liu, M. Tang, H. Yu, *J. Mater. Chem. A* **2021**, *9*, 8966.
[73] Y. Guo, H. Jin, Z. Qi, Z. Hu, H. Ji, L.-J. Wan, *Adv. Funct. Mater.* **2019**, *29*, 1807676.
[74] S. Ju, C. Yuan, J. Zheng, L. Yao, T. Zhang, G. Xia, X. Yu, *Energy Storage Mater.* **2022**, *52*, 524.
[75] S. Ju, J. Ye, H. Zhang, W. Wang, G. Xia, W. Cui, Y. Yang, H. Pan, X. Yu, *Energy Storage Mater.* **2023**, *56*, 1.
[76] Z. Lin, M. Mao, T. Lv, S. Li, Y.-S. Hu, H. Li, X. Huang, L. Chen, L. Suo, *Energy Storage Mater.* **2022**, *51*, 266.
[77] X. Zheng, Z. Wang, J. Li, L. Wei, *Sci. China Mater.* **2022**, *65*, 1463.
[78] M. Gorle, V. R. Jetti, *New J. Chem.* **2024**, *48*, 4020.
[79] W. Chu, S. He, S. Liu, X. Zhang, S. Li, H. Yu, *Chem. Commun.* **2022**, *58*, 11539.
[80] W. Jiang, Y. Bian, Y. Zhang, M. Lin, *IOP Conf. Ser.: Earth Environ. Sci.* **2021**, *692*, 032070.
[81] Q. Sun, L. Chai, X. Yang, W. Zhang, Z. Li, *J. Colloid Interface Sci.* **2025**, *677*, 284.
[82] J. Lv, G. Lai, T. Yang, X. Sun, F. Liu, W. Wu, M. Shi, G. Wang, K. Gao, X. Li, N. Chen, *Chem. Eng. J.* **2024**, *494*, 152811.
[83] Q. Zhou, D. Wang, Y. Lian, H. Zhang, J. Zhao, *Ceram. Int.* **2023**, *49*, 89862.
[84] Z. Hu, S. Xie, Y. Guo, Y. Ye, J. Zhang, S. Jin, H. Ji, *J. Energy Chem.* **2022**, *67*, 354.
[85] J. Wang, J. Xu, Z. Huang, G. Fan, *Fullerenes, Nanotubes Carbon Nanostruct.* **2021**, *29*, 39.
[86] W. Wang, Z. Cao, G. A. Elia, Y. Wu, W. Wahyudi, E. Abou-Hamad, A.-H. Emwas, L. Cavallo, L.-J. Li, J. Ming, *ACS Energy Lett.* **2018**, *3*, 2899.
[87] Y. Guo, Z. Hu, Y. Cui, J. Wang, S. Jin, Z. Peng, H. Ji, *Batteries Supercaps* **2022**, *5*, 202100355.
[88] S. Lysgaard, J. M. García Lastra, *J. Phys. Chem. C* **2021**, *125*, 16444.
[89] T. Tsuda, J. Sasaki, Y. Uemura, T. Kojima, H. Senoh, S. Kuwabata, *Chem. Commun.* **2022**, *58*, 1518.
[90] Z. Huang, W. Wang, W.-L. Song, M. Wang, H. Chen, S. Jiao, D. Fang, *Angew. Chem. Int. Ed.* **2022**, *61*, 202202696.
[91] S. Licht, J. Hwang, T. S. Light, R. Dillon, *J. Electrochem. Soc.* **1997**, *144*, 948.
[92] S. Licht, *J. Electrochem. Soc.* **1997**, *144*, L133.
[93] C. Xu, T. Diemant, X. Liu, S. Passerini, *Adv. Funct. Mater.* **2023**, *33*, 2214405.
[94] C. Xu, T. Diemant, X. Liu, S. Passerini, *Adv. Mater.* **2024**, *36*, 2400263.
[95] Y. Bian, W. Jiang, Y. Zhang, L. Zhao, X. Wang, Z. Lv, S. Zhou, Y. Han, H. Chen, M.-C. Lin, *ChemSusChem* **2022**, *15*, 202101398.
[96] R. Jay, A. L. Jadhav, L. W. Gordon, R. J. Messinger, *Chem. Mater.* **2022**, *34*, 4486.
[97] Y. Ai, S.-C. Wu, F. Zhang, X. Zhang, R. Li, Y. Lan, L. Cai, W. Wang, *Energy Storage Mater.* **2022**, *48*, 297.
[98] Y. Zhang, L. Ma, R. Tang, X. Zheng, X. Wang, Y. Dong, G. Kong, F. Zhao, L. Wei, *Int. J. Hydrogen Energy* **2021**, *46*, 4936.
[99] X. Zhang, H. Ma, J. Liu, J. Chen, H. Lu, Y. Huang, J. Wang, *Nano Res.* **2023**, *16*, 8159.
[100] X. Xiao, J. Tu, Z. Huang, S. Jiao, *Phys. Chem. Chem. Phys.* **2021**, *23*, 10326.

[101] Q. Zhou, X. Jiang, X. Zhang, D. Wang, G. Yang, H. Zhou, Y. Wu, F. Guo, M. Chen, G. Diao, L. Ni, *ChemSusChem* **2024**, *17*, 202400424.
[102] F. Wang, M. Jiang, T. Zhao, P. Meng, J. Ren, Z. Yang, J. Zhang, C. Fu, B. Sun, *Nano-Micro Lett.* **2022**, *14*, 169.
[103] H. Hao, T. Hutter, B. L. Boyce, J. Watt, P. Liu, D. Mitlin, *Chem. Rev.* **2022**, *122*, 8053.
[104] Z. Ma, Z. Qi, G. Song, S. Huang, Z. Du, J. Dong, C. Guan, P. Luo, P. Gan, B. Yu, B. Guo, J. Chen, M. Wang, J. Zhang, X. Li, J. Zhang, F. Li, *Adv. Funct. Mater.* **2024**, *34*, 2403101.
[105] X. Zheng, R. Tang, Y. Zhang, L. Ma, X. Wang, Y. Dong, G. Kong, L. Wei, *Sustain Energ Fuels* **2020**, *4*, 1630.
[106] X. Zhou, C. Wu, Z. Zhao, Y. Wang, Y. Yang, J. Guo, J. Wang, X. He, Y. Xiang, N. Han, J. Li, *Mater. Today Chem.* **2024**, *38*, 102055.
[107] Z. Huang, W. Wang, M. Kou, H. Lei, Y. Luo, S. Jiao, *J. Mater. Sci. Technol.* **2023**, *152*, 86.
[108] P. Chiochan, X. Yu, M. Sawangphruk, A. Manthiram, *Adv. Energy Mater.* **2020**, *10*, 2001285.
[109] Y.-Z. Sun, J.-Q. Huang, C.-Z. Zhao, Q. Zhang, *Sci. China: Chem.* **2017**, *60*, 1508.
[110] Z. Huang, S. Li, Z. Wang, W. Wang, H. Lei, S. Jiao, *Adv. Energy Mater.* **2023**, *13*, 2302464.
[111] Y. Long, H. Li, M. Ye, Z. Chen, Z. Wang, Y. Tao, Z. Weng, S.-Z. Qiao, Q.-H. Yang, *Energy Storage Mater.* **2021**, *34*, 194.
[112] Q. Ran, H. Shi, H. Meng, S.-P. Zeng, W.-B. Wan, W. Zhang, Z. Wen, X.-Y. Lang, Q. Jiang, *Nat. Commun.* **2022**, *13*, 576.
[113] Q. Ran, S.-P. Zeng, M.-H. Zhu, W.-B. Wan, H. Meng, H. Shi, Z. Wen, X.-Y. Lang, Q. Jiang, *Adv. Funct. Mater.* **2023**, *33*, 2211271.
[114] X. Zhang, S. Jiao, *Int. J. Miner., Metall. Mater.* **2022**, *29*, 896.
[115] H. Wang, S. Gu, Y. Bai, S. Chen, N. Zhu, C. Wu, F. Wu, *J. Mater. Chem. A* **2015**, *3*, 22677.
[116] H. Chen, H. Xu, B. Zheng, S. Wang, T. Huang, F. Guo, W. Gao, C. Gao, *ACS Appl. Mater. Interfaces* **2017**, *9*, 22628.
[117] S. He, J. Wang, X. Zhang, W. Chu, S. Zhao, D. He, M. Zhu, H. Yu, *J. Mater. Chem. A* **2023**, *11*, 17020.
[118] H. Jiao, S. Jiao, W.-L. Song, X. Xiao, D. She, N. Li, H. Chen, J. Tu, M. Wang, D. Fang, *Nano Res.* **2021**, *14*, 646.
[119] J. Smajic, S. Wee, F. R. F. Simoes, M. N. Hedhili, N. Wehbe, E. Abou-Hamad, P. M. F. J. Costa, *ACS Appl. Energy Mater.* **2020**, *3*, 6805.
[120] J. Lampkin, H. Li, L. Furness, R. Raccichini, N. Garcia-Araez, *ChemSusChem* **2020**, *13*, 3514.
[121] K. Zhang, T. H. Lee, J. H. Cha, R. S. Varma, J.-W. Choi, H. W. Jang, M. Shokouhimehr, *Sci. Rep.* **2019**, *9*, 13573.

Yu Wang received his B.S. degree from the School of Materials Science and Engineering of Taiyuan University of Technology in 2021. He is currently a postgraduate in the School of Materials Science and Engineering at Wuhan University of Technology. His research interests focus on molten salt aluminum-sulfur batteries.

Xiaolin Wu received his B.S. degree from the School of Materials and Chemical Engineering of Henan University of Urban Construction in 2022. He is currently a postgraduate in the School of Chemical Engineering at Zhengzhou University. His research interests focus on fast-charging materials for molten salt aluminum-sulfur batteries.

Jiashen Meng is now a specially appointed researcher at the School of Materials Science and Engineering, Wuhan University of Technology. He received his B.S. and Ph.D. degrees in materials science and engineering from Wuhan University of Technology in 2015 and 2020, respectively. In 2018–2019, he was a visiting Ph.D. student at Massachusetts Institute of Technology. In 2020–2023, he was a Boxin postdoctoral research fellow at Peking University. His current research focuses on developing new materials and chemical solutions for extreme batteries and spent battery recycling technologies.

Liqiang Mai is the Chair Professor of Materials Science and Engineering at WUT, Dean of the School of Materials Science and Engineering at WUT, and Fellow of the Royal Society of Chemistry. He received his Ph.D. from WUT in 2004 and carried out his postdoctoral research at the Georgia Institute of Technology in 2006–2007. He worked as an advanced research scholar at Harvard University and the University of California, Berkeley. His current research interests focus on new nanomaterials for electrochemical energy storage and micro/nano energy devices.